Tunable transmembrane chloride transport by bis-indolylureas

Cally J. E. Haynes,[a] Stephen J. Moore,[a] Jennifer R. Hiscock,[a] Igor Marques,[b] Paulo Jorge Costa,[b] Vítor Félix[b] and Philip A. Gale[a]*

Supplementary Information

Computational Details

All the Molecular Dynamics (MD) simulations were carried out with the General AMBER Force Field (GAFF)[i] using the following protocols.

Multi-conformational RESP charge fitting of the transporters. Since the bis-indolylureas transporters **4-12** present a relatively large conformational flexibility, we decided to use several distinct conformation of each transporter to calculate the atomic point charges by means of multi-conformational RESP charge fitting methodology.[ii] Initially, transporters **4-12** were geometry optimized at the HF/6-31G* level of theory using Gaussian09[iii] with a starting random conformation. Subsequently, parameters from GAFF[i] were assigned to the transporters and RESP atomic charges were fitted to the electrostatic potential obtained at the HF/6-31G* using 4 concentric layer of points per atom and 6 points per unit area (Gaussian IOP 6/33=2, 6/41=4, 6/42=6) in agreement with the methodology followed in the force field reference. Then, transporters **4-12** were submitted to a 1 ns molecular dynamics (MD) run in the gas phase at 1000 K using AMBER11,[iv] which allows a stochastic covering of the conformational space of the transporters, and saving a trajectory file composed of 10000 structures. All these structures were further minimized by molecular mechanics (MM), through 1000 steps of the steepest descent method, followed by the conjugate gradient method until a convergence criterion of 0.0001 kcal mol^{-1} was achieved. The MM minimized conformations of each transporter were then clustered by root-mean-square deviation (RMSD) similarity and 5 different and independent conformations were chosen for each transporter.

These 5 conformations were again geometry optimized at the HF/6-31G* level of theory and the electrostatic potential was calculated for each of them, allowing the calculation of multi-conformational RESP atomic point charges, using identical weights for all conformations.

Simulations in Water and Surface Area calculations. The lowest-energy conformations found in the previous step for transporters **4-12** were immersed in cubic boxes composed of 4311 SPC/E model water molecules.[v] The solvent was initially relaxed keeping the solute fixed with a harmonic restrain of 500 kcal mol^{-1} $Å^{-2}$, followed by a MM minimization off all the system. Subsequently, the system was heated to 300 K during 50 ps using the Langevin thermostat with a collision frequency of 1 ps^{-1} in an NVT ensemble. After 2.5 ns of equilibration in a NPT ensemble at 1 atm with isotropic pressure scaling using relaxation time of 2 ps, the data were collected during 30 ns for all transporters. The SHAKE[vi] algorithm was used in all solution simulations to constrain all bonds involving hydrogen atoms, thus allowing the usage of 2 fs time step. A 10 Å cut-off was used for the non-bonded van der Waals interactions. Frames were saved every 1.0 ps leading to a trajectory files containing 30000 structures. This process enables to sample the available conformations in solution at 300 K.

The polar surface area (PSA) was calculated taking into account only the polar atoms (N and O) of the bis-indolylurea transporters and the hydrogen atoms attached to them, using the Linear Combinations of Pairwise Overlaps (LCPO) algorithm[vii] as implemented in the *cpptraj* utility of Ambertools 1.5. For all transporters, the corresponding trajectories of the MD simulation in water were loaded and the 30000 total snapshots were read every 100 frames, leading to 300 conformations for each transporter. Thus, the reported PSA is the average of those 300 conformations. The total surface area (TSA) was calculated in the same way, but now taking into account all atoms of the transporters.

1-palmitoyl-2-oleoylphophatidylcholine (POPC) lipid parameterization. Although several force fields are available for lipids and suitable for phospholipid bilayer simulations, their default parameters usually are not suitable to describe arbitrary organic molecules such as transporters **4-12**, requiring parameter adaptation or development, which is not trivial. However, in 2007, Jójárt and Martinek[viii] reported the first pure POPC bilayer simulations using GAFF with promising results. Two other publications followed, expanding the GAFF use to lipid bilayers composed of DMPC / DOPC[ix] or simply of DOPC.[x] These developments opened the possibility for phospholipid bilayer

simulations with arbitrary organic molecules using the same force field without further parameterisation.

In the original Jójárt and Martinek work[viii] it was shown that the use of GAFF in a NPT ensemble underestimates the POPC area per lipid of a model membrane model composed of 128 lipids and 2985 TIP3P water molecules; while the use of this force field combined with surface tension (γ = 60 dyn cm^{-1} per bilayer) in a NPγT ensemble improves significantly the accuracy of the membrane biophysical parameters. The same was also shown for a DOPC bilayer.[x]

Very recently,[xi] we also used GAFF parameters to simulate POPC bilayers using different simulation conditions with two water models and a slightly different strategy was followed for the calculation of the lipid atomic point charges. Thus, 13 independent POPC conformations were taken and a muti-conformational RESP charge calculation was performed, but contrarily to Jójárt and Martinek, we did not impose any charge restraint to the different lipid structural entities: phosphate, choline and CH_2 lipid tails as described in reference viii. The results of this comprehensive computational study will be submitted to publication soon, but, very briefly, we found that simulations with a bilayer composed of 72 POPC lipids with 2242 SPC/E water molecules[v] in an NPγT ensemble (γ = 60 dyn cm^{-1} per bilayer, T = 310 K) in GROMACS 4.5.3 provides an average area per lipid of 65.55 Å^2, which is in excellent agreement with the available experimental values, 68.3 Å^2 and 66 Å^2, taken from references xii and xiii respectively.

Membrane/transporter systems setup and simulation protocol. A previously equilibrated bilayer, composed of 72 POPC lipid molecules (36 lipids each layer) and 4954 SPC/E water molecules[xi] was used. Transporters **4**, **7**, and **12** were immersed in the water slab, away (>10 Å) from the water/lipid interface. The systems were relaxed by molecular mechanics using 10000 steps of steepest descent minimization with a large harmonic restrain (200000 kJ mol^{-1} nm^{-2}) on the transporters in order to remove bad contacts between the water molecules and the transporters and then, a full MM minimization was performed to all systems. After the minimization, a short NVT molecular dynamics run of 50 ps at 310 K was performed keeping a 4000 kJ mol^{-1} nm^{-2} restraint on the transporter. Long MD simulations of 180 ns in a NPγT ensemble (γ = 60

dyn cm^{-1} per bilayer, T = 310 K) were then performed for all systems in triplicate, by giving three different seeds to the velocities generation algorithm. This gives a total 180 ns x 3 replicas x 3 systems = 1620 ns of simulation.

Additional simulations were also performed with transporters **4**, **7**, and **12** placed in the centre of the POPC bilayer. For this purpose, after their insertion in the membrane core, the system was minimized with a large harmonic restrain (200000 kJ mol^{-1} nm^{-2}) on the transporter, allowing the lipid tails to accommodate around them without membrane disruption. The following steps were similar to the ones with the transporters in the water phase, except that only a single replica was performed for each transporter.

Molecular Dynamics Settings. All simulations were performed with GROMACS 4.5.3.[xiv] The long-range electrostatic interactions under periodic boundary conditions (PBC) were described with the Particle Mesh Ewald (PME) method[xv] using a 10 Å cut-off with a grid spacing of 1.2 Å. The same cut-off was applied to Lennard-Jones interactions and the nonbonded pair list was updated every 20 fs. The temperature of the systems was maintained by independent coupling of the lipids and the water molecules to an external bath temperature of 310 K, using the Berendsen thermostat[xvi] with a coupling constant of 0.1 ps^{-1}. The pressure was controlled by the Berendsen barostat at 1 atm (coupling constant of 1.0 ps) and using a compressibility of 4.5×10^{-5} bar^{-1}, with the independent coupling of the *x*-, *y*- and *z*- vectors, and a surface tension of 60 dyn cm^{-1}. The covalent bonds to hydrogen atoms were constrained using the LINCS algorithm[xvii] allowing the use of a 2 fs time step.

Simulation analysis. The results were analysed using the GROMACS 4.5.3 tools or with in-house custom scripts.

Supporting Figures and extended discussion

Structure-activity relationship. Analysis of the $EC_{50\ 270\ s}$ and clogP values presented in Table 1, together with the chloride efflux data plotted in Figure 3, indicates that, as the length of the alkyl chain between the two indolylureas is increased from **4**–**9** there is a general increase in chloride transport activity. After this point, in transporters **10-12**, this

order is broken. In Figure S1 it is indeed possible to see that for the smaller transporters with experimentally determined $EC_{50\ 270\ s}$ (**7-9**), as the clogP values increase, the $EC_{50\ 270\ s}$ values decrease. This would be expected since, the more lipophilic (higher clogP) the compound, more easily they can be internalized in the membrane. However, another correlation is also evident from the plot presented in Figure S1, for the larger transporters **9-12**, the clogP values increase (as they become more lipophilic) with $EC_{50\ 270\ s}$ values.

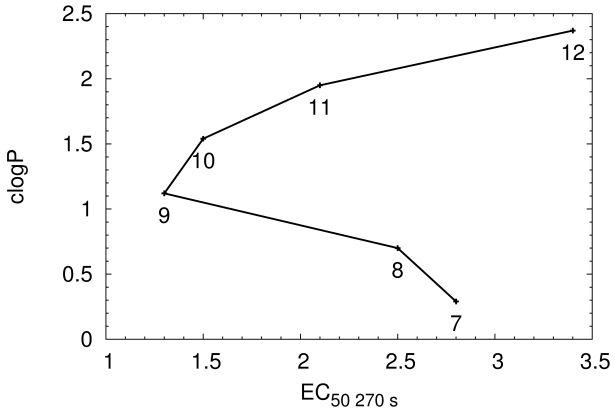

Figure S1 Plot of the calculated octanol:water partition coefficients (clogP) as a function of the experimental $EC_{50\ 270\ s}$ values.

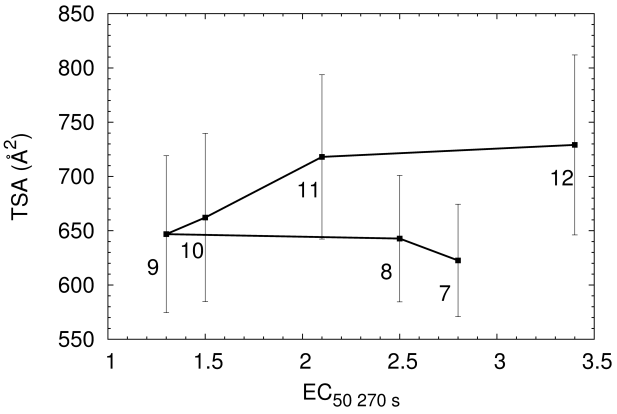

Figure S2 Plot of the calculated Total Surface Area (TSA / $Å^2$) as a function of the experimental $EC_{50\ 270\ s}$ values. The standard deviation values are plotted as error bars.

The same correlations were also found in the $EC_{50\ 270\ s}$ *vs.* Total Surface Area plot represented in Figure S2. For compounds **7-9**, the $EC_{50\ 270\ s}$ decreases as the TSA increases while for **9-12**, the $EC_{50\ 270\ s}$ values increase linearly with TSA ones.

Both clogP and TSA increase with increasing alkyl chain size leading to an increase of the chloride transport activity associated with the enlargement of the apolar aliphatic chain from **7** to **9**, while an inverse variation was observed going from **9** to **12**. It appears that n = 9 is the *turning point* where increasing the lipophilicity by increasing the chain length inhibits the $EC_{50\ 270\ s}$ transport activity. This is in total agreement with the hypothesis that the increased lipophilicity is only favourable for chloride transport until a certain chain size, after which, the longer chain receptors (n > 9) suffer reduced transport rates due to slower partitioning with the lipid bilayer as reported in the main text.

When the Polar Surface Area is plotted against $EC_{50\ 270\ s}$, as can be seen in Figure S3, another very nice correlation is evident for compounds **7**, **8**, **11**, **10** (in this order): remarkably, the calculated PSA does not decrease with increasing central alkyl chain length and, as the PSA becomes smaller, the $EC_{50\ 270\ s}$ decreases. In addition, the compounds **9** and **12** are clearly outliners in this correlation. This correlation indicates that, besides lipophilicity and chain size, the polar surface area accessible to the solvent and therefore, to POPC also plays an important role in the chloride transporter activity. This hypothesis is corroborated by the insertion mechanism of the receptors into POPC bilayers simulated by MD (see main text and further discussion presented below).

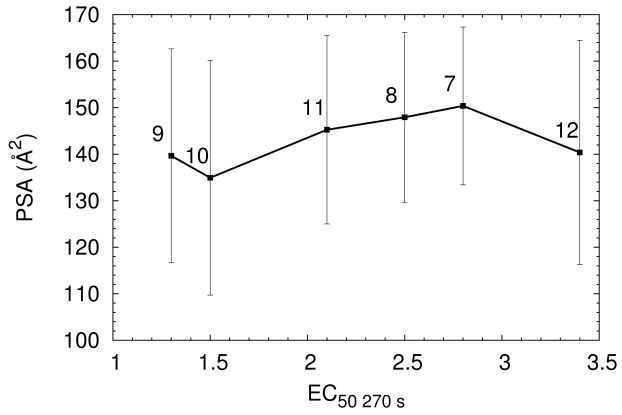

Figure S3 Plot of the calculated Polar Surface Area (TSA / $Å^2$) *versus* experimental $EC_{50\ 270\ s}$ values. The standard deviation values are plotted as error bars.

Molecular Dynamics Simulations. As mentioned in the main text, the receptors were immersed in the water slab, away (>10 Å) from the water/lipid interface and the

transporters were allowed to diffuse freely in the water phase. Figure S4 depicts the initial positions of the receptors **4**, **7** and **12** in these simulations.

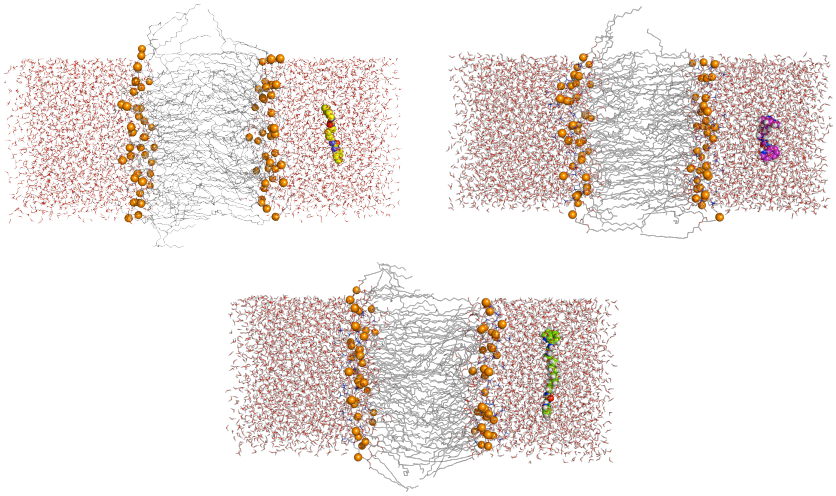

Figure S4 Initial configurations for the MD production runs carried out with transporters 4 (top, left), 7 (top, right), and 12 (bottom).

In order to increase the sampling of conformational space, 3 replicas for each receptor were performed. In some replicas, the transporters moved to the water/lipid interface during the course of the MD simulation. In order to evaluate this diffusion, the receptor was divided in 3 parts, according to Figure S5 where *head1* and *head2* refer to the centre of mass (COM) of the pyrrole ring from indole unit while *centre* is the central carbon atom in **7** or the COM of the central C-C bond in **4** and **12**. Then, we calculated the distances of these transporter geometrical points (*head1*, *head2* and *centre*) to the closest water/lipid interface, defined as the average z position of the phosphorus atoms in one layer. Positive values ($z > 0$) for all these three distances indicate that the receptor is in the water phase while negative values ($z < 0$) indicate that the receptor crossed the water/lipid interface ($z = 0$). These data are plotted in Figures S6, S7 and S8 while Table S1 reports the times when the crossing events occur.

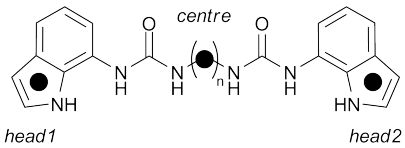

Figure S5 Representation of the bis-indolylureas transporters (*n* = 4, 7, and 12) with the location of the monitored reference points (black dots).

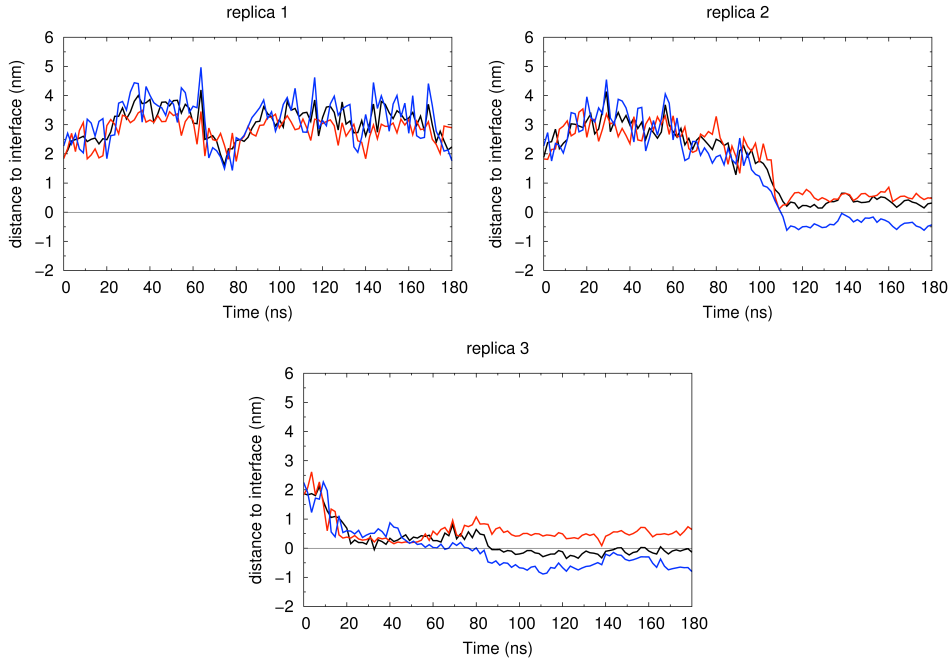

Figure S6 Distances to the interface (nm) of the transporter reference points *head1* (red), *head2* (blue) and *centre* (black) as a function of the simulation time (ns) for POPC system with **4.**

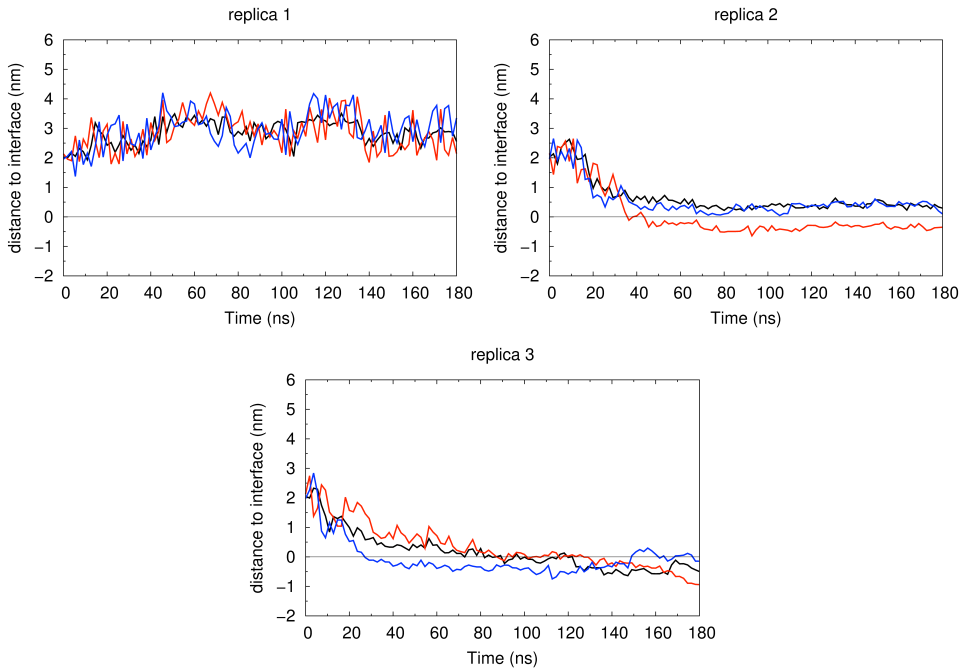

Figure S7 – Distances to the interface (nm) of the transporter reference points *head1* (red), *head2* (blue) and *centre* (black) as a function of the simulation time (ns) for POPC system with **7**.

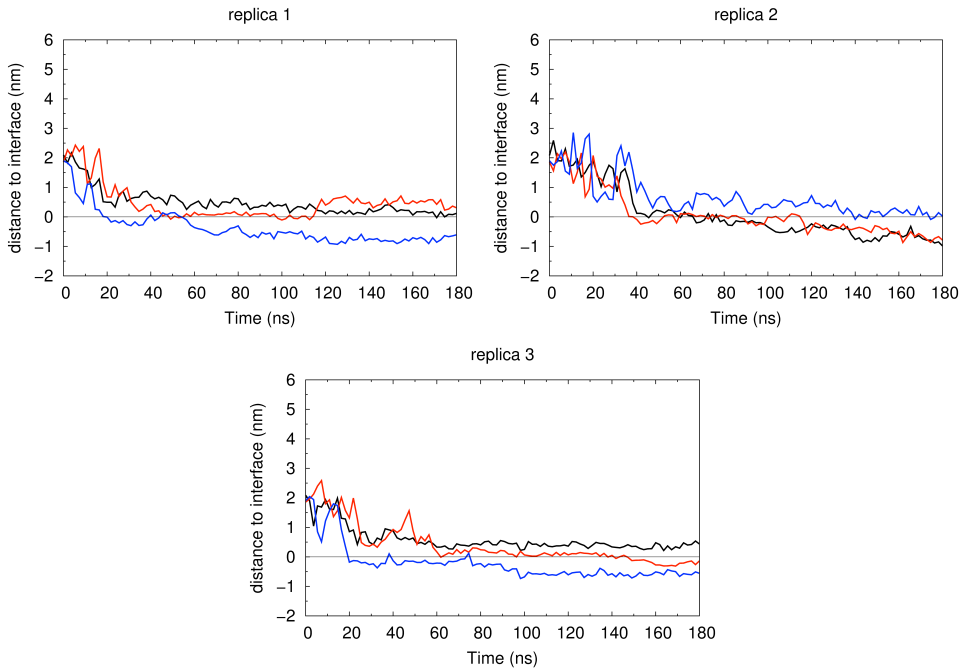

Figure S8– Distances to the interface (nm) of the transporter reference reference points *head1* (red), *head2* (blue) and *centre* (black) as a function of the simulation time (ns) for POPC system with **4-12.**

Table S1 – Simulation times (ns) of the crossing events for all replicas. *dnc* stands for "*does not cross*".

Transporter	Replica	*head1*	*head2*	*centre*
4	1	*dnc*	*dnc*	*dnc*
	2	*dnc*	107.3	*dnc*
	3	*dnc*	69.8	84.8
7	1	*dnc*	*dnc*	*dnc*
	2	34.6	*dnc*	*dnc*
	3	80.2	25.8	70.4
12	1	*dnc*	16.6	*dnc*
	2	36.3	*dnc*	40.2
	3	61.2	18.9	*dnc*

Starting by the POPC + **4** system, in the first replica, no internalization was observed as none of the receptor's parts comes closer than 1 nm of the interface during 180 ns of the MD simulation. Given the 10 Å cut-off used in our simulations for the *vdw* and electrostatic terms, this means that the membrane and **4** *don't see* each other. In replicas 2 and 3, the situation is different: in the second one, at ~107 ns, *head2* penetrates the lipid headgroups remaining below $z = 0$ until the end of simulation while *head1* and *centre* reference points are in the water phase during the entire time of simulation; in the third, *head1* and *centre* approach the interface, followed by *head2* which, after the first ~70 ns is internalized in the membrane. Subsequently, *ca.* 15 ns later, a pyrrole ring of one bis-indoylureia binding unit (*head2*), and the central carbon atom of the carbon chain (*centre*) definitively cross the headgroups level.

In the first replica of the POPC + **7** system, no internalization was observed. In the second replica, *head1* crosses the interface at ~35 ns settling below the water/lipid interface ($z < 0$) while *head2* and *centre* remain in water phase. The third replica is more

interesting because at the end of the simulation all parts of receptor **7** are internalized, starting by *head2*, followed by *centre* and *head1*.

For system POPC + **12** the crossing of the water/lipid interface by the transporter was observed in all replicas. In replica 1, only one pyrrole ring of an indole moitey (*head2*) crosses the interface remaining below the lipid heads while *head1* and *centre* touch the interface, crossing it only sporadically. In replica 2, the *head1* starts to cross the lipid headgroups at ~36 ns, followed by the centre of the carbon atom chain after the first ~40 ns of simulation. The second indole moiety (*head2*) remains outside the membrane. In replica 3, both *head* reference points cross the water/lipid interface while the *centre* one is positioned in the water phase for 180 ns of MD simulation.

The above results, illustrated by Figure 12 in the main text, show that in all replicas of all systems, the bis-indolylureas anion binding units, represented by reference points *heads* 1 and 2*,* are the first part of the transporters to interact and cross the interface in agreement with the previously found PSA *vs.* $EC_{50\ 270\ s}$ correlation.

Total internalization and bilayer crossing of the transporters was not observed during the simulation time of our unrestrained MD simulations. However, this is not surprising given the experimental timescale of that observation in the order of hundreds of seconds *vs.* hundreds of nanoseconds of our simulations. Figure S9 depicts representative snapshots taken at the end of the simulations for transporters **4**, **7**, and **12**.

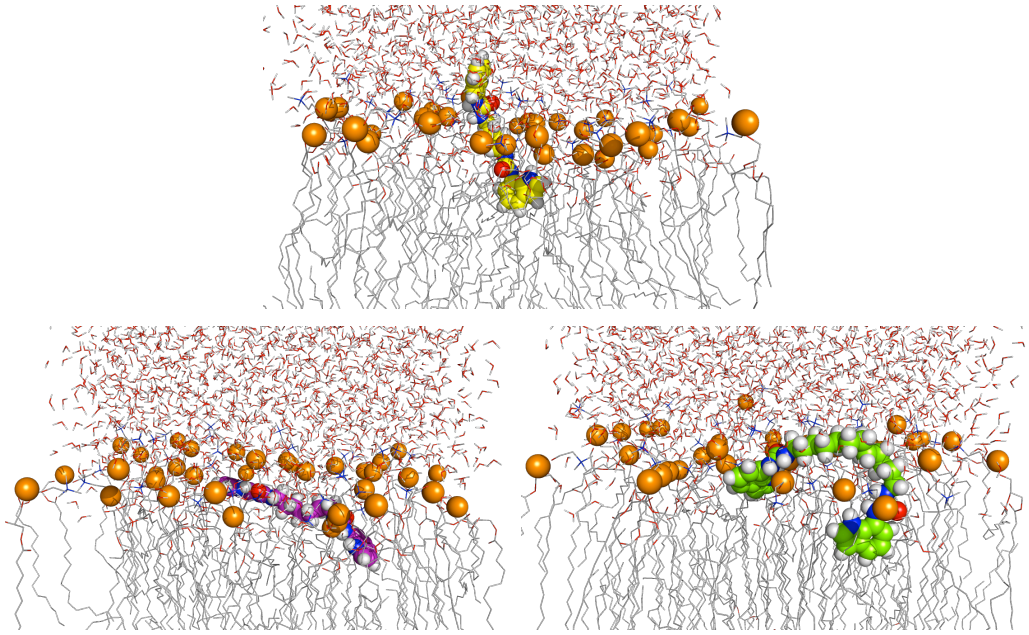

Figure S9– Representative snapshots (replica 3) taken at the end of the simulation time (180 ns) for transporters **4** (top, left), **7** (top, right), and **12** (bottom).

In order to evaluate the behaviour of these transporters inside the bilayer core and the impact caused by their complete internalisation in the structure of phospholipid bilayer, and since complete membrane crossing was not observed during the simulation time, simulations starting with each transporter in the centre of the membrane were also undertaken *via* a single replica. Again, the *z* position of *head1*, *head2* and *centre* the transporters was monitored together with the average *z* coordinate of the phosphorus atoms of each layer and is plotted in Figure S10 while Figure S11 shows the final snapshots of the simulations.

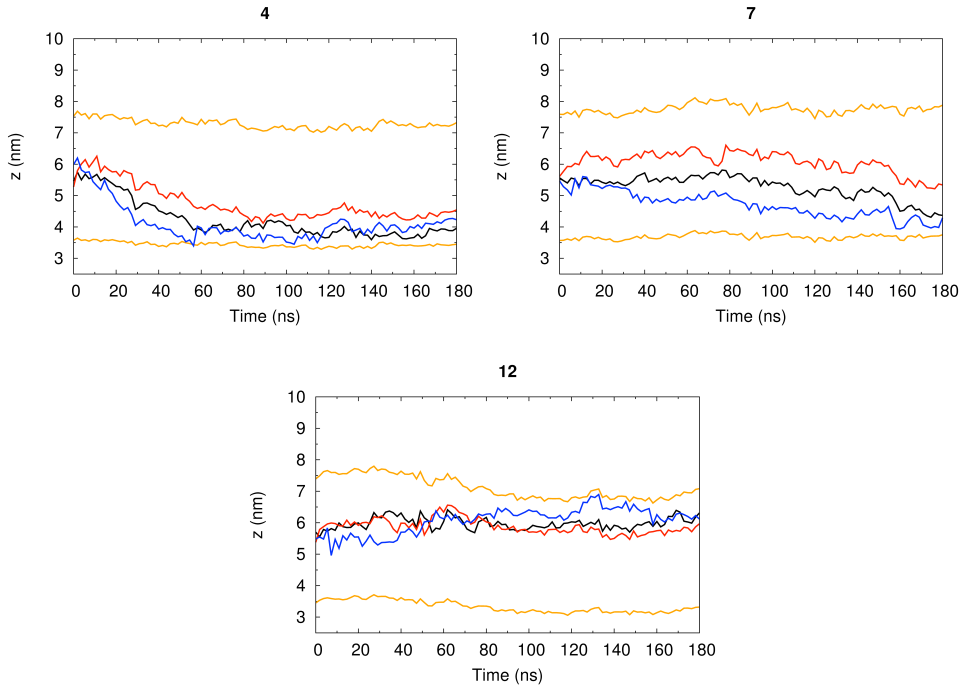

Figure S10– Evolution of the *z* position of the reference points *head1* (red), *head2* (blue) and *centre* (black) for **4** (top, left), **7** (top, right) and **12** (bottom, centre) along the simulation time when the transporter is initially positioned in the middle of the bilayer core. The average *z* coordinate of the phosphorus atoms of each layer is also plotted as orange lines.

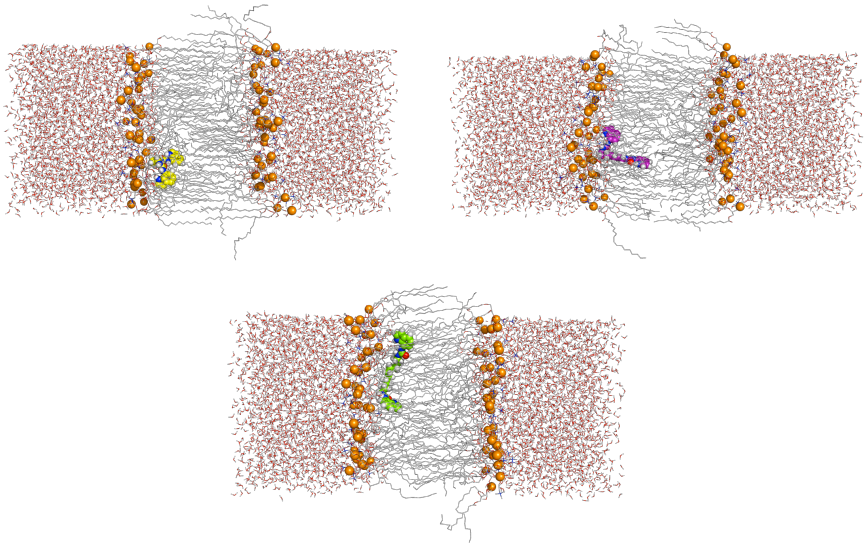

Figure S11– Snapshots taken at the end of the simulation time (180 ns) for transporters **4** (top, left), **7** (top, right), and **12** (bottom) starting from the core of the bilayer.

We calculated the mean-square displacement (MSD) along the bilayer normal (z) for the transporters inside the membrane, which is a measure of the average distance a molecule travels inside the membrane in the z direction. The MSD is defined according to

$$MSD\ (t) = \langle ||r_i(t) - r_i(0)||^2 \rangle$$

Where r_i is, in our case, the z position of the transporters centre of mass taken at $t = 0$ and $t = t$. The results are plotted in Figure S12.

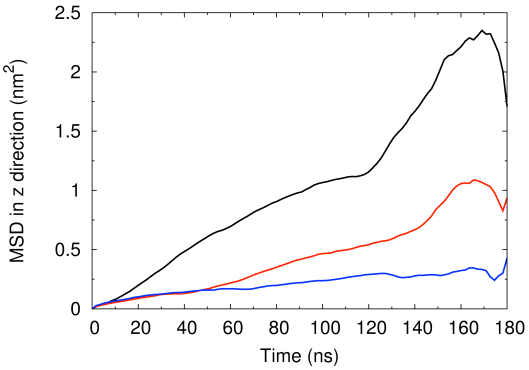

Figure S12– MSD along the bilayer normal (*z*) for transporters **4** (black line), **7** (red line) and **12** (blue line).

The results show that, from **4** to **12** the MSD values decrease, meaning that transporter **4** would in principle be faster than **7** and **12** to cross the phospholipid membrane. In contrast, the largest transporter **12** is the slowest. This is in agreement with the chain length *vs.* chloride transport activity hypothesis: longer transporters are not necessarily bad transporters but indeed take more time to be internalized into the membrane to start its action.

Supplementary experimental details

General Remarks

^{1}H NMR (300 MHz) and ^{13}C{^{1}H} NMR (75 MHz) were determined on a Bruker AV300 spectrometer. Chemical shifts for ^{1}H NMR are reported in parts per million (ppm), calibrated to the solvent peak set. The following abbreviations are used for spin multiplicity: s = singlet, d = doublet, t = triplet, m = multiplet. Chemical shifts for ^{13}C{^{1}H} NMR are reported in ppm, relative to the central line of a septet at δ = 39.52 ppm for DMSO-d_6. Infrared (IR) spectra were recorded on a Matterson Satellite (ATR). FTIR are reported in wavenumbers (cm^{-1}). HRMS(ES) spectra were recorded using a Bruker Apex III spectrometer and reported as *m/z* (relative intensity). All solvents and starting materials were purchased from commercial sources and used without further purification unless otherwise stated. Dry DCM was obtained by distillation over CaH_2 prior to use. POPC was supplied by Genzyme. Other lipids were purchased from Avanti. ^{1}H NMR titrations were performed by addition of aliquots of the putative anionic guest as the tetrabutylammonium (TBA) or tetraethylammonium (TEA) salt (0.15 M), in a solution of the receptor (0.01 M) in DMSO-d_6 H_2O 0.5 % to 0.01 M solution of the receptor. Data from the ^{1}H NMR titrations was fitted to the relevant binding model using WinEQNMR 2.[18] Chloride concentrations during transport experiments were determined using an Accumet chloride selective electrode.

Synthetic procedure

Bis-indolylureas **4-12** were synthesized according to the general procedure outlined below.

1,1'-(butane-1,4-diyl)bis(3-(1*H*-indol-7-yl)urea) 4

N-(1H-indol-7-yl)-1H-imidazole-1-carboxamide[19] (200 mg, ~0.8 mmol) was dissolved in dry DCM:DMF (50:1). 1,4-Diaminobutane (7.1 mg, 0.44 mmol) was added and the mixture was heated to reflux under N_2 and stirred overnight. The mixture was cooled and the white precipitate was collected by filtration. The solid was washed with 3 x 10 ml of water and 3 x 10 ml diethyl ether and dried under vacuum to give **1** as a white solid.

Yield: 43 mg (24 %); ^{1}H NMR (300 MHz, DMSO-d_6): δ= 10.68 (s, 2H, NH), 8.35 (s, 2H, NH), 7.29 (t, 2H, J=2.56 Hz, aromatic CH), 7.20 (d, 2H, J=7.68 Hz, aromatic CH), 7.07 (d, 2H, J=7.32 Hz, aromatic CH), 6.88 (t, 2H, J=7.68 Hz, aromatic CH), 6.39 (m, 2H, aromatic CH), 6.26 (t, 2H, J=5.49 Hz, aromatic CH), 3.18 (br m, 4H, 2x eq CH_2), 1.53 (br m, 4H, 2x eq CH_2); ^{13}C NMR (75 MHz, DMSO-d_6): δ=155.7 (CO), 129.1 (aromatic CH), 127.9 (aromatic CH), 124.9 (aromatic CH), 124.8 (aromatic CH), 119.1 (aromatic CH), 114.5 (aromatic CH), 111.8 (aromatic CH), 101.4 (aromatic CH), 27.4 (multiple overlapping CH_2); LRMS (ESI-): *m/z* = 403.1 ($[M-H]^-$); HRMS (ES): for $C_{22}H_{25}N_6O_2$ $[M + H]^+$ *m/z* = 405.2039 (calculated), 405.2032 (found); IR (film): ν= 3390 (indole NH stretching), 3310 (urea NH stretching); decomposes above 240 °C.

1,1'-(pentane-1,5-diyl)bis(3-(1*H*-indol-7-yl)urea) 5

Yield: 63 mg (34 %); ^{1}H NMR (300 MHz, DMSO-d_6): δ= 10.67 (s, 2H, NH), 8.32 (s, 2H, NH), 7.29 (t, 2H, J=2.56 Hz, NH), 7.20 (d, 2H, J=7.68 Hz, aromatic CH), 7.06 (d, 2H, J=6.95 Hz, aromatic CH), 6.88 (t, 2H, J=7.68 Hz, aromatic CH), 6.39 (m, 2H, aromatic CH), 6.24 (t, 2H, J=5.49 Hz, aromatic CH), 3.16 (q, 4H, J_1=6.59 Hz, J_2=6.22 Hz, 2x eq CH_2), 1.52 (m, 4H, 2x eq CH_2), 1.38 (m, 2H, CH_2); ^{13}C NMR (75 MHz, DMSO-d_6): δ= 155.6 (CO), 129.1 (aromatic CH), 127.8 (aromatic CH), 125.0 (aromatic CH), 124.8 (aromatic CH), 119.1 (aromatic CH), 114.5 (aromatic CH), 111.7 (aromatic CH), 101.4 (aromatic CH), 29.6 (CH_2), 23.8 (CH_2); LRMS (ESI+): *m/z* = 419.1 ($[M + H]^+$), 441.2 ($[M + Na]^+$); HRMS (ES): for $C_{23}H_{27}N_6O_2$ $[M + H]^+$ *m/z* = 419.2195 (calculated), 419.2190 (found); IR (film): ν= 3390 (indole NH stretching), 3390 (urea NH stretching), 3310 (urea NH stretching); decomposes above 240 °C.

1,1'-(hexane-1,6-diyl)bis(3-(1*H*-indol-7-yl)urea) 6

Yield: 75 mg (39 %); ^{1}H NMR (300 MHz, DMSO-d_6): δ= 10.67 (s, 2H, NH), 8.31 (s, 2H, NH), 7.29 (t, 2H, J= 2.93 Hz, NH), 7.20 (d, 2H, J=7.68 Hz,, aromatic CH), 7.06 (d, 2H, J=7.32 Hz, aromatic CH), 6.88 (t, 2H, J=7.68 Hz, aromatic CH), 6.40 (m, 2H, aromatic CH), 6.22 (t, 2H, J=5.49 Hz, aromatic CH), 3.15 (q, 4H, J_1=6.59 Hz, J_2=6.22 Hz, 2x eq CH_2), 1.50 (br m, 4H, 2x eq CH_2), 1.36 (br m, 4H, 2x eq CH_2); ^{13}C NMR (75 MHz, DMSO-d_6): δ= 155.6 (CO), 129.1 (aromatic CH), 127.8 (aromatic CH), 125.0 (aromatic CH), 124.8 (aromatic CH), 119.1 (aromatic CH), 114.5 (aromatic CH), 111.8 (aromatic CH), 101.4 (aromatic CH), 29.8 (CH_2), 26.2 (CH_2); LRMS (ESI+): *m/z* = 455.2 ([M + Na]$^+$); HRMS (ES): for $C_{24}H_{29}N_6O_2$ [M + H]$^+$ *m/z* = 433.2352 (calculated), 433.2348 (found); IR (film): ν= 3390 (indole NH stretching), 3310 (urea NH stretching); decomposes above 240 °C.

1,1'-(heptane-1,7-diyl)bis(3-(1*H*-indol-7-yl)urea) 7

Yield: 73 mg (37 %); ^{1}H NMR (300 MHz, DMSO-d_6): δ= 10.67 (br s, 2H, NH), 8.30 (s, 2H, NH), 7.29 (t, 2H, J=2.93 Hz, NH), 7.20 (d, 2H, J=8.05 Hz, aromatic CH), 7.05 (d, 2H, J=7.32 Hz, aromatic CH), 6.88 (t, 2H, J=7.68 Hz, aromatic CH), 6.39 (m, 2H, aromatic CH), 6.21 (t, 2H, J=5.85 Hz, aromatic CH), 3.14 (q, 4H, J_1= 6.59 Hz, J_2=6.22 Hz, 2x eq CH_2), 1.49 (m, 4H, 2x eq CH_2), 1.34 (br m, 6H, 3 x CH_2); ^{13}C NMR (75 MHz, DMSO-d_6): δ= 155.6 (CO), 129.1 (aromatic CH), 127.8 (aromatic CH), 125.0 (aromatic CH), 124.8 (aromatic CH), 119.1 (aromatic CH), 114.5 (aromatic CH), 111.7 (aromatic CH), 29.8 (CH_2), 28.6 (CH_2), 26.4 (CH_2); LRMS (ESI+): *m/z* = 470.3 ([M + Na]$^+$); HRMS (ES+): for $C_{25}H_{31}N_6O_2$ [M + H]$^+$ *m/z* = calculated 447.2508, found 447.2498; IR (film): ν= 3390 (indole NH stretching), 3320 (urea NH stretching); decomposes above 240 °C.

1,1'-(octane-1,8-diyl)bis(3-(1*H*-indol-7-yl)urea) 8

Yield: 70 mg (34 %); ^{1}H NMR (300 MHz, DMSO-d_6): δ= 10.67 (br s, 2H, NH), 8.29 (s, 2H, NH), 7.30 (t, 2H, J=2.56 Hz, NH), 7.20 (d, 2H, J=7.68 Hz, aromatic CH), 7.04 (d, 2H, J=7.32 Hz, aromatic CH), 6.88 (t, 2H, J=7.68 Hz, aromatic CH), 6.39 (m, 2H, aromatic CH), 6.20 (t, 2H, J= 5.85 Hz, aromatic CH), 3.13 (q, 4H, J_1=6.59 Hz, J_2=5.85 Hz, 2x eq CH_2), 1.48 (m, 4H, 2x eq CH_2), 1.32 (br m, 8H, 4x CH_2); ^{13}C NMR (75 MHz, DMSO-d_6): δ= 155.6 (CO), 129.1 (aromatic CH), 127.8 (aromatic CH), 124.8 (aromatic CH), 119.2 (aromatic CH), 114.5 (aromatic CH), 111.7 (aromatic CH), 108.7 (aromatic CH), 101.4 (aromatic CH), 29.8 (CH_2), 28.8 (CH_2), 26.40 (CH_2); LRMS (ESI+): *m/z* = 483.2 ($[M + Na]^+$); HRMS (ES): for $C_{26}H_{33}N_6O_2$ $[M + H]^+$ 461.2665 (calculated), 461.2659 (found); IR (film): ν= 3390 (indole NH stretching), 3320 (urea NH stretching); decomposes above 240 °C.

1,1'-(nonane-1,9-diyl)bis(3-(1H-indol-7-yl)urea) 9

Yield: 104 mg (66 %); ^{1}H NMR (300 MHz, DMSO-d_6): δ= 10.68 (s, 2H, NH), 8.35 (s, 2H, NH), 7.29 (t, 2H, J=2.56 Hz, aromatic CH), 7.20 (d, 2H, J=7.68 Hz, aromatic CH), 7.07 (d, 2H, J=7.32 Hz, aromatic CH), 6.88 (t, 2H, J=7.68 Hz, aromatic CH), 6.39 (m, 2H, aromatic CH), 6.26 (t, 2H, J=5.49 Hz, aromatic CH), 3.14 (q, J= 6.6 Hz, 4H, 2x eq CH_2), 1.46 (br m, 4H, 2x eq CH_2), 1.31 (br s, 10 H, 5x CH_2); ^{13}C NMR (75 MHz, DMSO-d_6): δ= 155.6 (CO), 129.1 (aromatic CH), 127.8 (aromatic CH), 125.0 (aromatic CH), 124.8 (aromatic CH), 119.1 (aromatic CH), 114.5 (aromatic CH), 111.715 (aromatic CH), 101.4 (aromatic CH), 29.8 (CH_2), 29.1 (CH_2), 28.8 (CH_2), 26.4 (CH_2); LRMS (ESI+): *m/z* = 497.2 ($[M + Na]^+$); HRMS (ES): for $C_{27}H_{34}N_6O_2$ *m/z* = $[M + H]^+$ calculated 475.2821, found 475.2820; IR (film): ν= 3390 (indole NH stretching), 3320 (urea NH stretching); decomposes above 227 °C.

1,1'-(decane-1,10-diyl)bis(3-(1*H*-indol-7-yl)urea) 10

Yield: 97 mg (60 %); ^{1}H NMR (300 MHz, DMSO-d_6): δ= 10.67 (s, 2H, NH), 8.35 (s, 2H, NH), 7.29 (t, 2H, J=2.56 Hz, aromatic CH), 7.20 (d, 2H, J=7.68 Hz, aromatic CH), 7.07 (d, 2H, J=7.32 Hz, aromatic CH), 6.88 (t, 2H, J=7.68 Hz, aromatic CH), 6.39 (m, 2H, aromatic CH), 6.26 (t, 2H, J=5.49 Hz, aromatic CH), 3.14 (q, J= 6.6 Hz, 4H, 2x eq CH_2), 1.46 (br m, 4H, 2x eq CH_2), 1.31 (br s, 12 H, 6x CH_2); ^{13}C NMR (75 MHz, DMSO-d_6): δ= 155.6 (CO), 129.1 (aromatic CH), 127.8 (aromatic CH), 125.0 (aromatic CH), 124.8 (aromatic CH), 119.1 (aromatic CH), 114.5 (aromatic CH), 111.7 (aromatic CH), 101.4 (aromatic CH), 29.8 (CH_2), 29.0 (CH_2), 28.8 (CH_2), 26.4 (CH_2); LRMS (ESI+): *m/z*= 511.2 ([M + Na]$^+$); HRMS (ES): for $C_{28}H_{37}N_6O_2$ *m/z* = [M + H]$^+$ calculated 489.2978, found 489.2982; IR (film): ν= 3390 (indole NH stretching), 3320 (urea NH stretching); decomposes above 225 °C.

1,1'-(undecane-1,11-diyl)bis(3-(1H-indol-7-yl)urea) 11

Yield; 137 mg (82 %); ^{1}H NMR (300 MHz, DMSO-d_6): δ= 10.67 (s, 2H, NH), 8.35 (s, 2H, NH), 7.29 (t, 2H, J=2.56 Hz, aromatic CH), 7.20 (d, 2H, J=7.68 Hz, aromatic CH), 7.07 (d, 2H, J=7.32 Hz, aromatic CH), 6.88 (t, 2H, J=7.68 Hz, aromatic CH), 6.39 (m, 2H, aromatic CH), 6.26 (t, 2H, J=5.49 Hz, aromatic CH), 3.14 (q, J= 6.6 Hz, 4H, 2x eq CH_2), 1.46 (br m, 4H, 2x eq CH_2), 1.31 (br s, 14 H, 7x CH_2); ^{13}C NMR (75 MHz, DMSO-d_6): δ= 155.6, (CO), 129.1 (aromatic CH), 127.8, (aromatic CH), 125.0 ((aromatic CH), 119.1 (aromatic CH), 114.5 (aromatic CH), 111.7 (aromatic CH), 101.4 (aromatic CH), 29.8 (CH_2), 29.0 (CH_2), 28.8 (CH_2), 26.4 (CH_2); LRMS (ESI+) *m/z*= 525.3 ([M + Na]$^+$, 16.99%), 503.3 ([M + H]$^+$, 4.97%); LRMS (ESI-): *m/z* = 501.7 ([M-H]$^-$); HRMS (ES+): for $C_{29}H_{38}N_6O_2Na$ [M + Na]$^+$ *m/z* = calculated 525.2954, found 525.2957; IR (film): ν= 3390 (indole NH stretching), 3320 (urea NH stretching); decomposes above 215 °C.

1,1'-(dodecane-1,12-diyl)bis(3-(1*H*-indol-7-yl)urea) 12

Yield: 125 mg (77 %); ^{1}H NMR (300 MHz, DMSO-d_6): δ= 10.67 (s, 2H, NH), 8.35 (s, 2H, NH), 7.29 (t, 2H, J=2.56 Hz, aromatic CH), 7.20 (d, 2H, J=7.68 Hz, aromatic CH), 7.07 (d, 2H, J=7.32 Hz, aromatic CH), 6.88 (t, 2H, J=7.68 Hz, aromatic CH), 6.39 (m, 2H, aromatic CH), 6.26 (t, 2H, J=5.49 Hz, aromatic CH), 3.14 (q, J= 6.6 Hz, 4H, 2x eq CH_2), 1.46 (br m, 4H, 2x eq CH_2), 1.31 (br s, 14 H, 7x CH_2); ^{13}C NMR (75 MHz, DMSO-d_6): δ= 155.6 (CO), 129.1 (aromatic CH), 127.8 (aromatic CH), 125.0 (aromatic CH), 124.8 (aromatic CH), 119.1 (aromatic CH), 114.5 (aromatic CH), 111.7 (aromatic CH), 101.4 (aromatic CH), 29.8 (CH_2), 29.0 (CH_2), 26.4 (CH_2); LRMS (ESI-) *m/z*= 515.2 ([M-H]$^-$); HRMS (ES): for $C_{30}H_{41}N_6O_2$ [M + H]$^+$ *m/z* = calculated 517.3291, found 517.3281; IR (film): ν= 3390 (indole NH stretching), 3320 (urea NH stretching); decomposes above 221 °C.

1-Butyl-3-(1H-indol-7-yl)urea[20] 13

N-(1H-indol-7-yl)-1H-imidazole-1-carboxamide[1] (0.142g, 0.628mmol) was suspended in DCM (100mL). 1-butylamine (2.00mL, 20.2mmol) was added and the reaction mixture refluxed at 50°C for 18 hours. The reaction mixture was reduced *in vacuo* to yield an oil. The oil was triturated with hexane (50mL) and ether (10mL) to yield a white solid, which was removed by filtration. The solid was purified by column chromatography (10% methanol in DCM) to yield a white solid.

Yield: 97 mg (67 %); ^{1}H NMR (300 MHz, DMSO-d_6): δ= 10.69 (br. s., 1 H, NH), 8.35 (s, 1 H, NH), 7.30 (t, *J*=2.78 Hz, 1 H, ArCH), 7.20 (d, *J*=8.08 Hz, 1 H, Ar CH), 7.07 (d, *J*=7.58 Hz, 1 H, Ar CH), 6.88 (t, *J*=7.83 Hz, 1 H, Ar CH), 6.39 (t, *J*=2.27 Hz, 1 H, Ar CH), 6.21 (t, *J*=5.56 Hz, 1 H, NH), 3.14 (app. q, 2 H, CH_2), 1.41 - 1.51 (m, 2 H, CH_2), 1.34 (m, 2 H, CH_2), 0.91 (t, *J*=7.33 Hz, 3 H, CH_3); ^{13}C NMR (75 MHz, DMSO-d_6): δ= 155.7 (CO), 129.1 (ArC), 127.8 (ArC), 125.0 (ArC), 124.8 (ArCH), 119.1 (ArCH), 114.5 (ArCH), 111.6 (ArCH), 101.5 (ArCH), 39.0 (CH_2), 31.9 (CH_2), 19.6 (CH_2), 13.7 (CH_3);

LRMS (ESI+) *m/z*= 232.3 ($[M+H]^+$), 254.2 ($[M+Na]^+$), 485.3 ($[2M+Na]^+$); HRMS (ES): for $C_{13}H_{17}N_3ONa$ $[M+Na]^+$ *m/z* = calculated 254.1264, found 254.1262; IR (film): ν= 3370 (s, NH stretch), 3270 (m, NH stretch), 2960 (s, CH stretch), 2940 (s, CH stretch), 2870 (m, CH stretch), 1650 (s, C=O stretch); M_p: 136 ºC.

1-Pentyl-3-(1H-indol-7-yl)urea 14

N-(1H-indol-7-yl)-1H-imidazole-1-carboxamide[1] (0.137g, 0.606mmol) was suspended in DCM (200mL).1-pentylamine (0.65mL, 5.63mmol) was added to the reaction mixture which was refluxed at 50°C for 66 hours. The reaction mixture was reduced *in vacuo* and then purified by column chromatography (10% ethyl acetate in DCM) to yield an off-white solid.

Yield: 60 mg (40 %); ^{1}H NMR (300 MHz, DMSO-d_6): δ= 10.66 (br. s., 1 H, NH), 8.27 (s, 1 H, NH), 7.30 (br. s., 1 H, ArCH), 7.20 (d, *J*=8.08 Hz, 1 H, ArCH), 7.04 (d, *J*=7.58 Hz, 1 H, ArCH) 6.88 (t, *J*=7.83 Hz, 1 H, ArCH), 6.39 (br. s., 1 H, ArCH), 6.19 (t, *J*=5.56 Hz, 1 H, NH) 3.09 - 3.17 (m, 2 H, CH_2), 1.51-1.44 (m, 2 H, CH_2), 1.25 - 1.36 (m, 4 H, 2xCH_2) 0.89 (t, *J*=6.57 Hz, 3 H, CH_3); ^{13}C NMR (75 MHz, DMSO-d_6): δ= 155.6 (CO), 129.2 (ArC), 127.9 (ArC), 125.0 (ArC), 124.8 (ArCH), 119.1 (ArCH), 114.6 (ArCH), 111.8 (ArCH), 111.8 (ArCH), 101.5 (ArCH), 39.4 (CH_2), 29.5 (CH_2), 28.6 (CH_2), 21.9 (CH_2), 13.9 (CH_3); LRMS (ESI+) *m/z*= 246.2 ($[M+H]^+$), 268.2 ($[M+Na]^+$), 513.2 ($[2M+Na]^+$); HRMS (ES): for $C_{14}H_{19}N_3ONa$ $[M+Na]^+$ *m/z* = calculated 268.1420, found 268.1416; IR (film): ν= 3390 (s, NH stretch), 3310 (s, NH stretch), 2950 (w, CH stretch), 2930 (s, CH stretch), 2870 (m, CH stretch), 1630 (s, C=O stretch); M_p: 137 ºC.

1-Hexyl-3-(1H-indol-7-yl)urea 15

N-(1H-indol-7-yl)-1H-imidazole-1-carboxamide[1] (0.140g, 0.619mmol) was suspended in DCM (100mL).1-hexylamine (2.50mL,18.92mmol) was added to the reaction mixture

which was refluxed at 50°C for 16 hours. The reaction mixture was washed with water (3x50mL) and the organic fraction reduced *in vacuo* and then purified by column chromatography (10% methanol in DCM) to yield an off-white solid

Yield: 104 mg (65 %); ^{1}H NMR (300 MHz, DMSO-d_6): δ= 10.65 (br. s., 1 H, NH), 8.27 (s, 1 H, NH), 7.29 (t, *J*=2.80Hz, 1 H, ArCH), 7.20 (d, *J*=8.08 Hz, 1 H, ArCH), 7.04 (d, *J*=7.58 Hz, 1 H, ArCH), 6.82 - 6.92 (m, 1 H, ArCH) 6.39 (dd, *J*=3.03, 2.02 Hz, 1 H, ArCH), 6.18 (t, *J*=5.60Hz, 1 H, NH), 3.06 - 3.18 (m, 2 H, CH_2) 1.40 - 1.54 (m, 2 H, CH_2) 1.23 - 1.37 (m, 6 H, 3xCH_2), 0.87 (t, *J*=7.60 Hz, 2 H, CH_3); ^{13}C NMR (75 MHz, DMSO-d_6): δ= 155.7 (CO), 129.2 (ArC), 127.9 (ArC), 125.0 (ArC), 124.8 (ArCH), 119.1 (ArCH), 114.6 (ArCH), 111.8 (ArCH), 101.5 (ArCH), 39.4 (CH_2), 31.0 (CH_2), 29.7 (CH_2), 26.1 (CH_2), 22.1 (CH_2), 13.9 (CH_3); LRMS (ESI+) *m/z*= 260.2 ($[M+H]^+$), 282.2 ($[M+Na]^+$), 541.4 ($[2M+Na]^+$); HRMS (ES): for $C_{15}H_{21}N_3ONa$ $[M+Na]^+$ *m/z* = calculated 282.1577, found 282.1574; IR (film): ν= 3410 (s, NH stretch), 3350 (m, NH stretch), 3290 (w, NH stretch), 2950 (w, CH stretch), 2930 (s, CH stretch), 2860 (m, CH stretch), 1630 (s, C=O stretch); M_p: 136 ºC.

1-Heptyl-3-(1H-indol-7-yl)urea 16

N-(1H-indol-7-yl)-1H-imidazole-1-carboxamide[1] (0.107g, 0.473mmol) was suspended in DCM (40mL).1-heptylamine (0.50mL, 3.38mmol) was added to the reaction mixture which was refluxed at 50°C for 66 hours. The reaction mixture was reduced *in vacuo* and then purified by column chromatography (10% methanol in DCM) to yield a white solid.

Yield: 67 mg (52 %); ^{1}H NMR (300 MHz, DMSO-d_6): δ= 10.70 (br. s., 1 H, NH), 8.33 (s, 1 H, NH), 7.29 (br. s., 1 H, ArCH), 7.19 (d, *J*=7.58 Hz, 1 H, ArCH), 7.06 (d, *J*=7.58 Hz, 1 H, ArCH), 6.88 (t, *J*=7.58 Hz, 1 H, ArCH), 6.39 (br. s., 1 H, ArCH), 6.23 (t, *J*=5.05 Hz, 1 H, NH), 3.13 (m, 2 H, CH_2), 1.47 (m, 2 H, CH_2), 1.20 - 1.35 (m, 8 H, 4xCH_2), 0.87

(t, *J*=6.06 Hz, 3 H, CH_3); ^{13}C NMR (75 MHz, DMSO-d_6): δ= 155.7 (CO), 129.1 (ArC), 127.8 (ArC), 125.0 (ArC), 124.8 (ArCH), 119.1 (ArCH), 114.5 (ArCH), 111.7 (ArCH), 101.4 (ArCH), 39.4 (CH_2), 31.3 (CH_2), 29.8 (CH_2), 28.5 (CH_2), 26.4 (CH_2), 22.1 (CH_2), 13.9 (CH_3); LRMS (ESI+) *m/z*= 274.2 ($[M+H]^+$), 296.2 ($[M+Na]^+$); HRMS (ES): for $C_{16}H_{23}N_3ONa$ $[M+Na]^+$ *m/z* = calculated 296.1733, found 296.1736; IR (film): ν= 3380 (s, NH stretch), 3310 (s, NH stretch), 2950 (w, CH stretch), 2930 (s, CH stretch), 2850 (m, CH stretch), 1630 (s, C=O stretch); M_p: 128 ºC.

1-Octyl-3-(1H-indol-7-yl)urea[2] 17

N-(1H-indol-7-yl)-1H-imidazole-1-carboxamide[1] (0.159g, 0.703mmol) was suspended in DCM (200mL).1-octylamine (0.50mL, 3.03mmol) was added to the reaction mixture which was refluxed at 50°C for 17 hours. The reaction mixture was washed with water (150mL) and then purified by column chromatography (10% methanol in DCM) to yield a white solid.

Yield: 79 mg (39 %); ^{1}H NMR (300 MHz, DMSO-d_6): δ= 10.65 (br. s., 1 H, NH), 8.27 (s, 1 H, NH), 7.29 (t, *J*=2.53 Hz, 1 H, ArCH), 7.20 (d, *J*=7.58 Hz, 1 H, ArCH), 7.03 (d, *J*=7.58 Hz, 1 H, ArCH), 6.82 - 6.94 (m, 1 H, ArCH), 6.33 - 6.44 (m, 1 H, ArCH), 6.18 (t, *J*=5.31 Hz, 1 H, NH), 3.13 (q, *J*=6.23 Hz, 2 H, CH_2), 1.41 - 1.53 (m, 2 H, CH_2), 1.20 - 1.36 (m, 10 H, 5xCH_2), 0.86 (t, *J*=5.60 Hz, 3 H, CH_3); ^{13}C NMR (75 MHz, DMSO-d_6): δ= 155.6 (CO), 129.2 (ArC), 127.9 (ArC), 125.0 (ArC), 124.8 (ArCH), 119.1 (ArCH), 114.6 (ArCH), 111.8 (ArCH), 101.5 (ArCH), 39.4 (CH_2), 31.2 (CH_2), 29.8 (CH_2), 28.8 (CH_2), 28.7 (CH_2), 26.4 (CH_2), 26.4 (CH_2), 22.1 (CH_2), 13.9 (CH_3); LRMS (ESI+) *m/z*= 288.3 ($[M+H]^+$), 310.3 ($[M+Na]^+$), 597.5 ($2M+Na]^+$); HRMS (ES): for $C_{17}H_{25}N_3ONa$ $[M+Na]^+$ *m/z* = calculated 310.1890, found 310.1892; IR (film): ν = 3390 (s, NH stretch), 3310 (s, NH stretch), 2950 (w, CH stretch), 2920 (s, CH stretch), 2850 (m, CH stretch), 1630 (s, C=O stretch); M_p: 134 ºC (lit. 137 ºC).

1-Nonyl-3-(1H-indol-7-yl)urea 18

N-(1H-indol-7-yl)-1H-imidazole-1-carboxamide[1] (0.092g, 0.407mmol) was suspended in DCM (100mL).1-nonylamine (0.50mL, 2.73mmol) was added to the reaction mixture which was refluxed at 50°C for 5 hours. The reaction mixture was reduced *in vacuo* and then purified by column chromatography (10% ethyl acetate in DCM) to yield a white solid.

Yield: 81 mg (66 %); ^{1}H NMR (300 MHz, DMSO-d_6): δ= 10.66 (br. s., 1 H, NH), 8.27 (s, 1 H, NH), 7.29 (t, *J*=2.53 Hz, 1 H, ArCH), 7.20 (d, *J*=8.08 Hz, 1 H, ArCH), 7.04 (d, *J*=7.58 Hz, 1 H, ArCH), 6.88 (t, *J*=7.58 Hz, 1 H, ArCH), 6.39 (br. s., 1 H, ArCH), 6.19 (t, *J*=5.56 Hz, 1 H, NH), 3.03 - 3.17 (m, 2 H, CH_2), 1.42 - 1.52 (m, 2 H, CH_2), 1.27 (s, 12 H, 6xCH_2), 0.86 (t, *J*=6.32 Hz, 3 H, CH_3); ^{13}C NMR (75 MHz, DMSO-d_6): δ= 155.6 (CO), 129.2 (ArC), 127.9 (ArC), 125.0 (ArC), 124.8 (ArCH), 119.1 (ArCH), 114.5 (ArCH), 111.7 (ArCH), 101.4 (ArCH), 39.4 (CH_2), 31.3 (CH_2), 29.8 (CH_2), 29.0 (CH_2), 28.8 (CH_2), 26.4 (CH_2), 22.1 (CH_2), 13.9 (CH_2); LRMS (ESI+) *m/z*= 302.3 ($[M+H]^+$), 324.3 ($[M+Na]^+$), 625.5 ($[2M+Na]^+$); HRMS (ES): for $C_{18}H_{27}N_3ONa$ $[M+Na]^+$ *m/z* = calculated 324.2046, found 324.2045; IR (film): ν= 3390 (s, NH stretch), 3300 (s, NH stretch), 2950 (w, CH stretch), 2920 (s, CH stretch), 2850 (m, CH stretch), 1630 (s, C=O stretch); M_p: 130 ºC.

1-Decyl-3-(1H-indol-7-yl)urea 19

N-(1H-indol-7-yl)-1H-imidazole-1-carboxamide[1] (0.113g, 0.499mmol) was suspended in DCM (50mL).1-decylamine (0.50mL, 2.50mmol) was added to the reaction mixture which was refluxed at 50°C for 18 hours. The reaction mixture was reduced *in vacuo* and sonicated in water for 0.5 hours. The resulting solid was removed by filtration and sonicated in DCM for 0.25 hours and then purified by column chromatography (10% methanol in DCM) to yield a cream coloured solid.

Yield: 99 mg (79 %); ^{1}H NMR (300 MHz, DMSO-d_6): δ= 10.67 (br. s., 1 H, NH), 8.31 (s, 1 H, NH), 7.29 (t, *J*=2.53 Hz, 1 H, ArCH), 7.19 (d, *J*=7.58 Hz, 1 H, ArCH), 7.06 (s, 1 H, ArCH), 6.83 - 6.93 (m, 1 H, ArCH), 6.35 - 6.42 (m, 1 H, ArCH), 6.20 (t, *J*=5.56 Hz, 1 H, NH), 3.07 - 3.18 (m, 2 H, CH_2), 1.40 - 1.52 (m, 2 H, CH_2), 1.17 - 1.34 (m, 14 H, 7xCH_2), 0.86 (t, *J*=6.82 Hz, 3 H, CH_3); ^{13}C NMR (75 MHz, DMSO-d_6): δ= 155.6 (CO), 129.1 (ArC), 127.8 (ArC), 125.0 (ArC), 124.8 (ArCH), 119.1 (ArCH), 114.5 (ArCH), 111.7 (ArCH), 101.4 (ArCH), 39.4 (CH_2), 31.3 (CH_2), 29.8 (CH_2), 29.1 (CH_2), 29.0 (CH_2), 28.8 (CH_2), 28.7 (CH_2), 26.4 (CH_2), 22.1 (CH_2), 13.9 (CH_3); LRMS (ESI+) *m/z*= 316.3 ([M+H]$^+$), 338.3 ([M+Na]$^+$), 653.6 (2M+Na]$^+$); HRMS (ES): for $C_{19}H_{29}N_3ONa$ [M+Na]$^+$ *m/z* = calculated 338.2203, found 338.2203; IR (film): ν= 3380 (s, NH stretch), 3310 (s, NH stretch), 2950 (w, CH stretch), 2920 (s, CH stretch), 2850 (m, CH stretch), 1630 (C=O stretch); M_p: 126 ºC.

1-Undecyl-3-(1H-indol-7-yl)urea 20

N-(1H-indol-7-yl)-1H-imidazole-1-carboxamide[1] (0.113 g, 0.499 mmol) was suspended in DCM (50 mL).1-undecylamine (0.54 mL, 2.50 mmol) was added to the reaction mixture which was refluxed at 50 °C overnight. The reaction mixture was reduced *in vacuo* and sonicated in water for 0.5 hours. The resulting solid was removed by filtration and sonicated in DCM for 0.25 hours and then purified by column chromatography (10% methanol in DCM) to yield an off-white solid.

Yield: 85 mg (52 %); ^{1}H NMR (300 MHz, DMSO-d_6): δ= 10.67 (br. s., 1 H, NH), 8.31 (s, 1 H, NH), 7.29 (t, *J*=2.53 Hz, 1 H, ArCH), 7.19 (d, *J*=7.58 Hz, 1 H, ArCH), 7.06 (s, 1 H, ArCH), 6.83 - 6.93 (m, 1 H, ArCH), 6.35 - 6.42 (m, 1 H, ArCH), 6.20 (t, *J*=5.56 Hz, 1 H, NH), 3.07 - 3.18 (m, 2 H, CH_2), 1.40 - 1.52 (m, 2 H, CH_2), 1.17 - 1.34 (m, 14 H, 7xCH_2), 0.86 (t, *J*=6.82 Hz, 3 H, CH_3); ^{13}C NMR (75 MHz, DMSO-d_6): δ= 155.6 (CO), 129.2 (ArC), 127.9 (ArC), 125.0 (ArC), 124.8 (ArCH), 119.1 (ArCH), 114.5 (ArCH),

111.7 (ArCH), 101.4 (ArCH), 39.4 (CH_2), 31.3 (CH_2), 29.8 (CH_2), 29.1 (CH_2), 29.0 (2xCH_2), 28.8 (CH_2), 28.7 (CH_2), 26.4 (CH_2), 22.1 (CH_2), 13.9 (CH_3); LRMS (ESI+) *m/z*= 330.3 ($[M+H]^+$), 352.3 ($[M+Na]^+$), 681.6 ($2M+Na]^+$); HRMS (ES): for $C_{20}H_{31}N_3ONa$ $[M+Na]^+$ *m/z* = calculated 352.2359, found 352.2364; IR (film): ν= 3380 (s, NH stretch), 3310 (s, NH stretch), 2950 (w, CH stretch), 2920 (s, CH stretch), 2850 (m, CH stretch), 1630 (C=O stretch); M_p: 126 ºC.

1-Dodecyl-3-(1H-indol-7-yl)urea 21

N-(1H-indol-7-yl)-1H-imidazole-1-carboxamide[1] (0.113 g, 0.499 mmol) was suspended in DCM (50 mL). 1-dodecylamine (0.57 mL, 2.50 mmol) was added to the reaction mixture which was refluxed at 50°C overnight. The reaction mixture was reduced *in vacuo* and sonicated in water for 0.5 hours. Resulting solid was removed by filtration and sonicated in DCM for 0.25 hours and then purified by column chromatography (10% methanol in DCM) to yield an off-white solid.

Yield: 96 mg (56 %); ^{1}H NMR (300 MHz, DMSO-d_6): δ= 10.66 (br. s., 1 H, NH), 8.27 (s, 1 H, NH), 7.29 (br. s., 1 H, ArCH), 7.20 (d, *J*=7.58 Hz, 1 H, ArCH), 7.04 (d, *J*=7.07 Hz, 1 H, ArCH), 6.83 - 6.91 (m, 1 H, ArCH), 6.39 (br. s., 1 H, ArCH), 6.18 (t, *J*=5.31 Hz, 1 H, NH), 3.12 (m, Hz, 2 H, CH_2), 1.45 (m, 2 H, CH_2), 1.15 - 1.35 (m, 18 H, 9xCH_2), 0.85 (t, *J*=6.57 Hz, 3 H, CH_3); ^{13}C NMR (75 MHz, DMSO-d_6): δ= 155.6 (CO), 129.2 (ArC), 127.9 (ArC), 125.0 (ArC), 124.8 (ArCH), 119.1 (ArCH), 114.5 (ArCH), 111.7 (ArCH), 101.4 (ArCH), 39.4 (CH_2), 31.3 (CH_2), 29.8 (CH_2), 29.1 (2xCH_2), 29.0 (2xCH_2), 28.8 (CH_2), 28.7 (CH_2), 26.4 (CH_2), 22.1 (CH_2), 13.9 (CH_3); LRMS (ESI+) *m/z*= 344.3 ($[M+H]^+$), 366.3 ($[M+Na]^+$), 687.7 ($2M+Na]^+$); HRMS (ES): for $C_{21}H_{33}N_3ONa$ $[M+Na]^+$ *m/z* = calculated 366.2516, found 366.2518; IR (film): ν= 3390 (s, NH stretch), 3300 (s, NH stretch), 2960 (w, CH stretch), 2920 (s, CH stretch), 2850 (m, CH stretch), 1630 (s, C=O stretch); M_p: 126 ºC.

Anion transport studies

Preparation of vesicles

A lipid film was formed from a chloroform solution of the desired lipid (and cholesterol if applicable) under reduced pressure and dried under vacuum for at least 4 hours. The lipid film was rehydrated by vortexing with a NaCl solution (489 mM, buffered to pH 7.2 with 5 mM sodium phosphate salts). The lipid suspension was then subjected to nine freeze-thaw cycles and allowed to age for 30 min at room temperature before extruding 25 times through a 200 nm polycarbonate membrane. The resulting unilamellar vesicles were dialyzed against the external medium to remove unencapsulated NaCl.

Chloride transport assays

Unilamellar vesicles containing NaCl, prepared as described above, were suspended in 489 mM $NaNO_3$ solution buffered to pH 7.2 with 5 mM sodium phosphate salts. The lipid concentration per sample was 1 mM. A DMSO solution of the carrier molecule (10 mM) was added to start the experiment and the chloride efflux was monitored using a chloride selective electrode. At 5 min, the vesicles were lysed with 50 μl of polyoxyethylene(8)lauryl ether (0.232 mM in 7:1 water:DMSO v/v) and a total chloride reading was taken at 7 min.

Nitrate pulse assay

Unilamellar POPC vesicles containing 489 mM NaCl solution buffered to pH 7.2 with 5 mM sodium phosphate salts, prepared as described above, were suspended in 167 mM Na_2SO_4 solution buffered to pH 7.2 with 5 mM sodium phosphate salts. The lipid concentration per sample was 1 mM. A DMSO solution of the carrier molecule (10 mM) was added to start the experiment and chloride efflux was monitored using a chloride selective electrode. At 2 min, $NaNO_3$ solution (1.2 M in 167 mM Na_2SO_4 buffered to pH

7.2 with 5 mM sodium phosphate salts) was added so that the outer solution contained 40 mM $NaNO_3$. At 7 min, the vesicles were lysed with 50 μl of polyoxyethylene(8)lauryl ether (0.232 mM in 7:1 water:DMSO *v/v*) and a total chloride reading was taken at 9 min. An analogous assay was used to investigate the bicarbonate transport properties, pulsing in 1.2 M $NaHCO_3$ with all solutions buffered to pH 7.2 with 20 mM sodium phosphate salts.

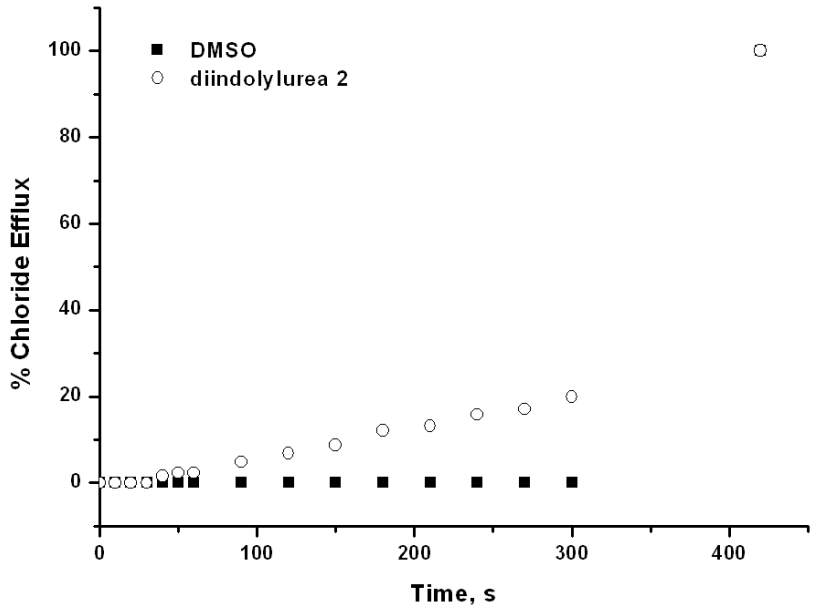

Figure S13 Chloride efflux promoted by diindolylurea 2 (4 mol % w.r.t. lipid) from unilamellar POPC vesicles loaded with 489 mM NaCl buffered to pH 7.2 with 5 mM sodium phosphate salts. The vesicles were suspended in 489 mM $NaNO_3$ buffered to pH 7.2 with 5 mM sodium phosphate salts. At the end of the experiment the vesicles were lysed by the addition of detergent to calibrate 100 % chloride efflux. Each point represents the average of 3 trials.

Transport mechanism determination

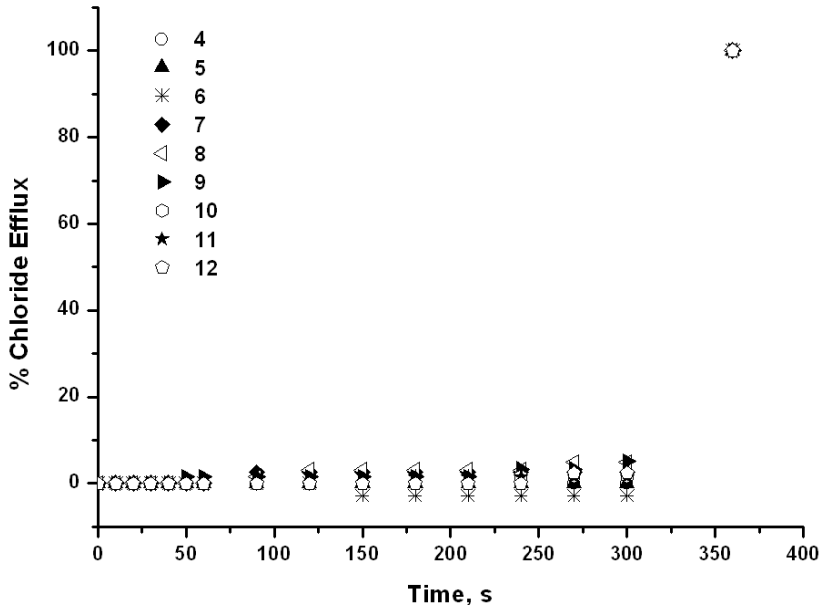

Figure S14 Chloride efflux promoted by receptors **4**-**12** (2 mol % w.r.t. lipid) from unilamellar POPC vesicles loaded with 489 mM NaCl buffered to pH 7.2 with 5 mM sodium phosphate salts. The vesicles were suspended in 167 mM Na_2SO_4 buffered to pH 7.2 with 5 mM sodium phosphate salts. At the end of the experiment the vesicles were lysed by the addition of detergent to calibrate 100 % chloride efflux. Each point represents the average of 3 trials.

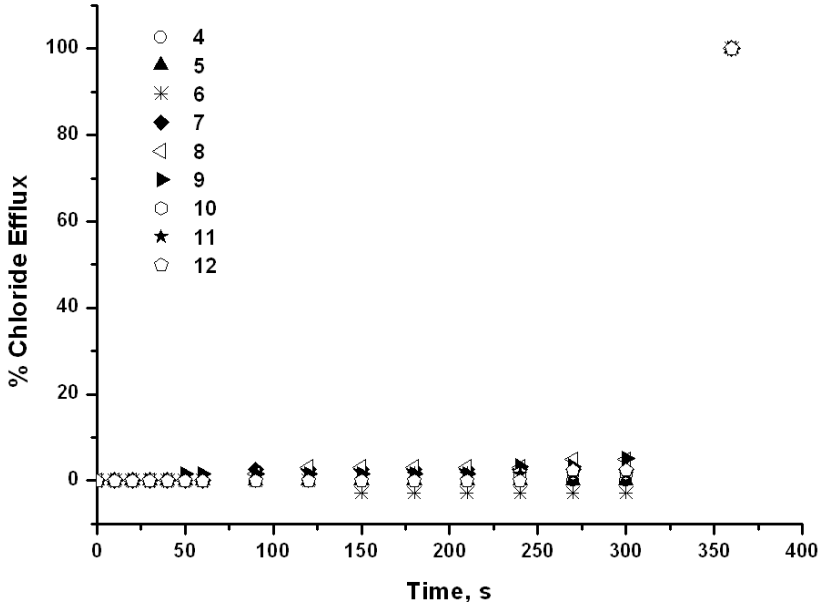

Figure S15 Chloride efflux promoted by receptors 4-12 (2 mol % w.r.t. lipid) from unilamellar POPC vesicles loaded with 489 mM NaCl buffered to pH 7.2 with 20 mM sodium phosphate salts. The vesicles were suspended in 167 mM Na_2SO_4 buffered to pH 7.2 with 20 mM sodium phosphate salts. At t = 120 s a pulse of $NaHCO_3$ was added such that the final HCO_3^- concentration was 40 mM. At the end of the experiment the vesicles were lysed by the addition of detergent to calibrate 100 % chloride efflux. Each point represents the average of 3 trials.

The Hill analysis

The Hill equation may be used to describe the relationship between drug concentration (C) and observed effect (E). This can be applied to anion transport by studying the relationship between the receptor concentration (C) and the observed chloride efflux at an arbitrary point, chosen in this case to be after 270 s (E). The Hill equation (**Equation 1**) is shown below.

$$E = E_{max}C^n / (EC_{50}{}^n + C^n)$$

Equation 1 The form of the Hill equation used in this work, where EC_{50} is the receptor cocentration for which 50 % of the maximum effect is observed and n is the Hill coefficient of sigmoidality.

The concentration of receptor added to the transport assay was varied; this was plotted against the observed chloride efflux after 270 s, and the data was fitted to **Equation 1** using Origin®, yielding calculated values of n and EC_{50}. The data for this process is shown below. For receptors that achieved less than 50 % total chloride efflux after 270 s at a concentration of 4 mol% with respect to lipid the analysis was not completed as the receptor was judged to be too inactive.

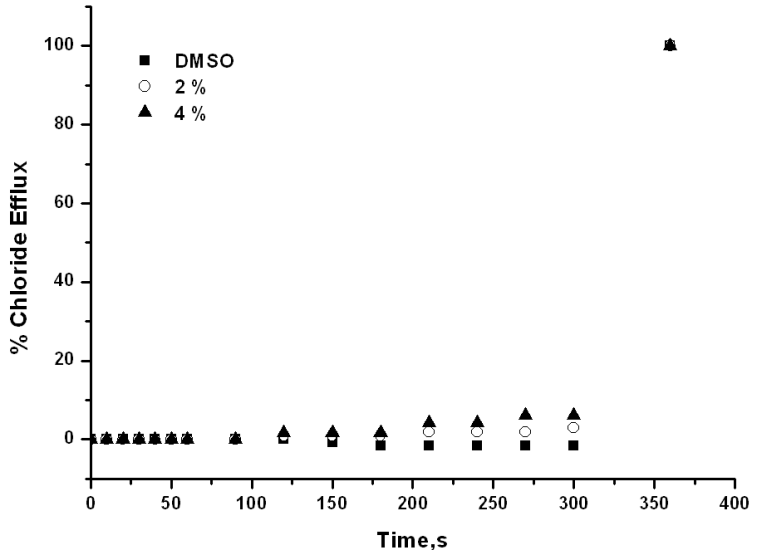

Figure S16 Chloride efflux mediated by various concentrations (mol% w.r.t. lipid) of receptor **4** from unilamellar POPC vesicles loaded with 489 mM NaCl buffered to pH 7.2 with 5 mM sodium phosphate salts. The vesicles were suspended in 489 mM $NaNO_3$ buffered to pH 7.2 with 5 mM sodium phosphate salts. At the end of the experiment the vesicles were lysed by the addition of detergent to calibrate 100 % chloride efflux. Each point represents the average of 3 trials.

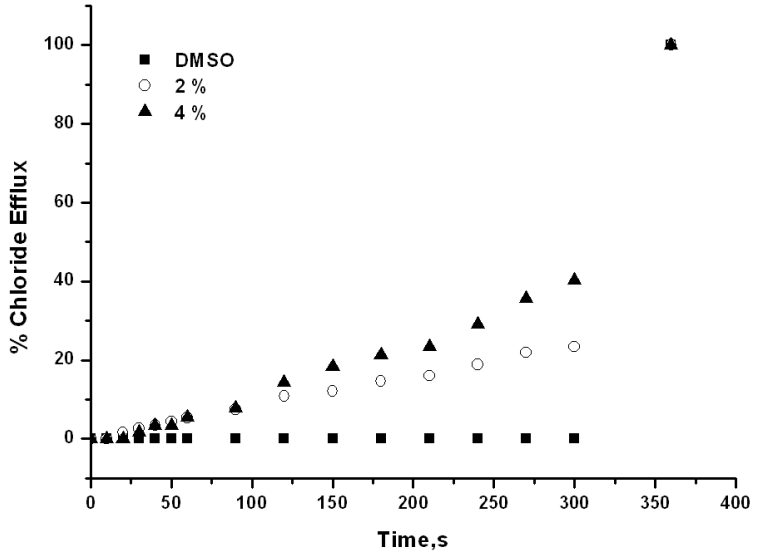

Figure S17 Chloride efflux mediated by various concentrations (mol% w.r.t. lipid) of receptor **5** from unilamellar POPC vesicles loaded with 489 mM NaCl buffered to pH 7.2 with 5 mM sodium phosphate salts. The vesicles were suspended in 489 mM $NaNO_3$ buffered to pH 7.2 with 5 mM sodium phosphate salts. At the end of the experiment the vesicles were lysed by the addition of detergent to calibrate 100 % chloride efflux. Each point represents the average of 3 trials.

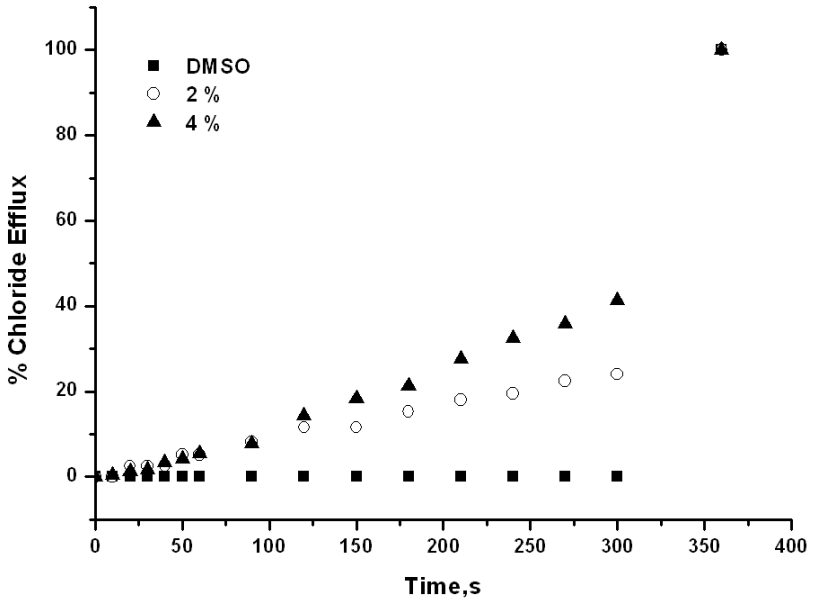

Figure S18 Chloride efflux mediated by various concentrations (mol% w.r.t. lipid) of receptor **6** from unilamellar POPC vesicles loaded with 489 mM NaCl buffered to pH 7.2 with 5 mM sodium phosphate salts. The vesicles were suspended in 489 mM $NaNO_3$ buffered to pH 7.2 with 5 mM sodium phosphate salts. At the end of the experiment the vesicles were lysed by the addition of detergent to calibrate 100 % chloride efflux. Each point represents the average of 3 trials.

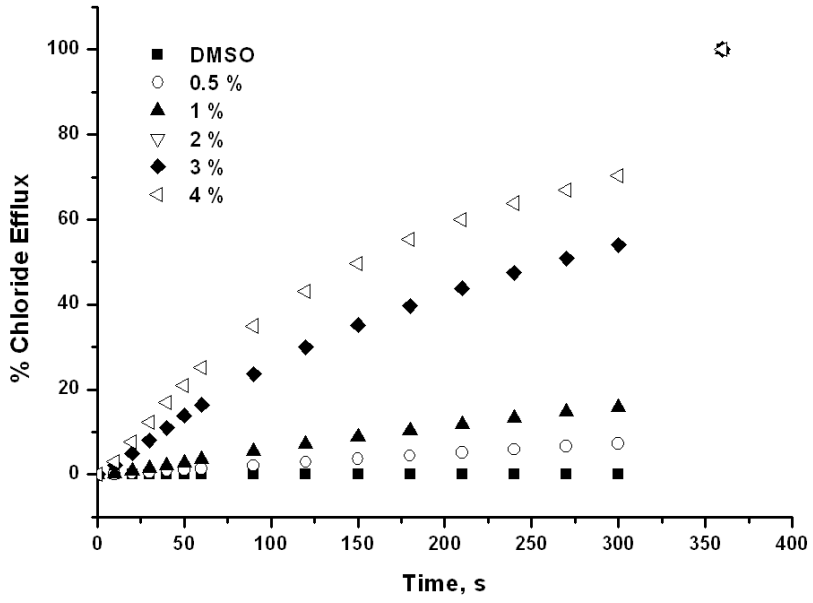

Figure S19 Chloride efflux mediated by various concentrations (mol% w.r.t. lipid) of receptor **7** from unilamellar POPC vesicles loaded with 489 mM NaCl buffered to pH 7.2 with 5 mM sodium phosphate salts. The vesicles were suspended in 489 mM $NaNO_3$ buffered to pH 7.2 with 5 mM sodium phosphate salts. At the end of the experiment the vesicles were lysed by the addition of detergent to calibrate 100 % chloride efflux. Each point represents the average of 3 trials.

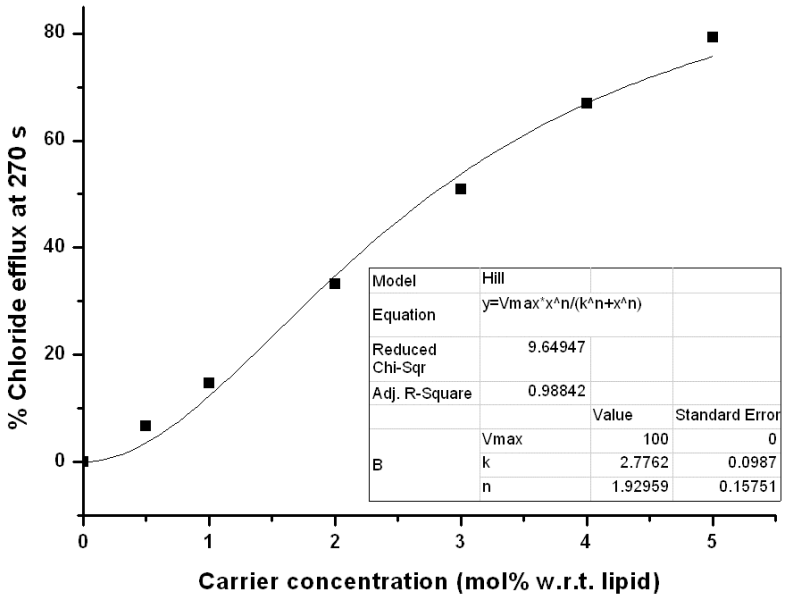

Figure S20 Hill plot for the Cl^-/NO_3^- antiport mediated by receptor **7** after 270 s, where k = EC_{50}, V_{max} = the maximum observable efflux (set to 100 %) and *n* is the Hill coefficient.

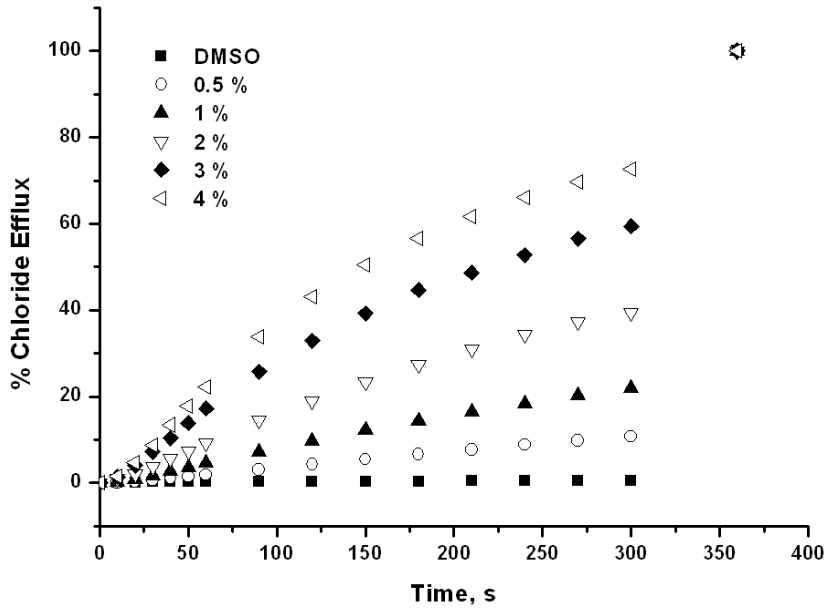

Figure S21 Chloride efflux mediated by various concentrations (mol% w.r.t. lipid) of receptor **8** from unilamellar POPC vesicles loaded with 489 mM NaCl buffered to pH 7.2 with 5 mM sodium phosphate salts. The vesicles were suspended in 489 mM $NaNO_3$ buffered to pH 7.2 with 5 mM sodium phosphate salts. At the end of the experiment the vesicles were lysed by the addition of detergent to calibrate 100 % chloride efflux. Each point represents the average of 3 trials.

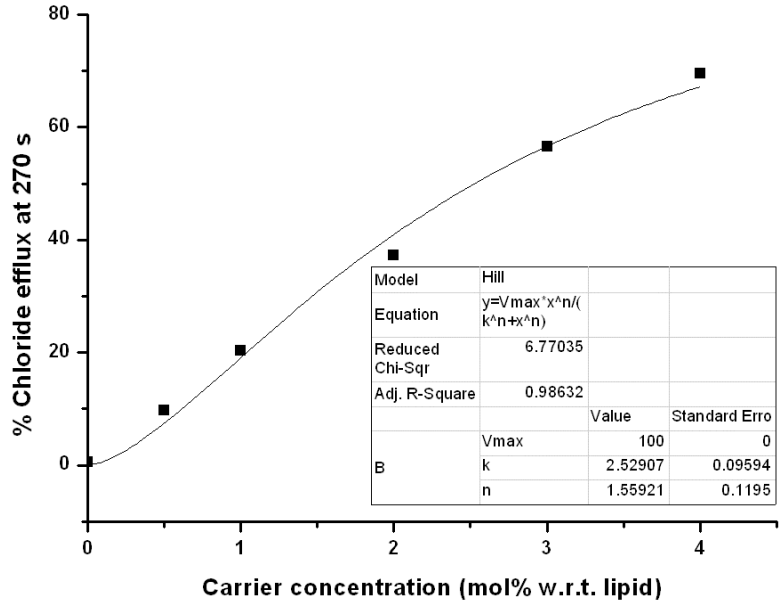

Figure S22 Hill plot for the Cl^-/NO_3^- antiport mediated by receptor **8** after 270 s, where k = EC_{50}, V_{max} = the maximum observable efflux (set to 100 %) and *n* is the Hill coefficient.

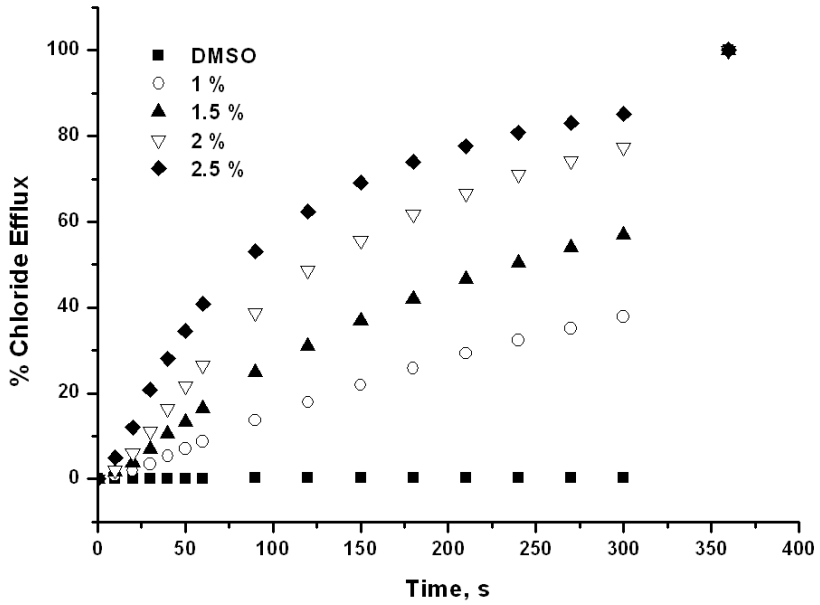

Figure S23 Chloride efflux mediated by various concentrations (mol% w.r.t. lipid) of receptor **9** from unilamellar POPC vesicles loaded with 489 mM NaCl buffered to pH 7.2 with 5 mM sodium phosphate salts. The vesicles were suspended in 489 mM $NaNO_3$ buffered to pH 7.2 with 5 mM sodium phosphate salts. At the end of the experiment the vesicles were lysed by the addition of detergent to calibrate 100 % chloride efflux. Each point represents the average of 3 trials.

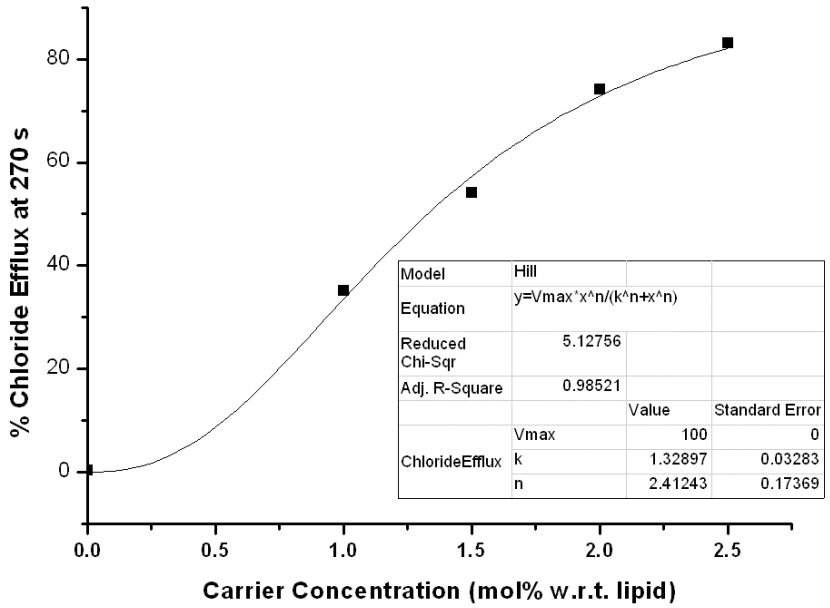

Figure S24 Hill plot for the Cl^-/NO_3^- antiport mediated by receptor **9** after 270 s, where k = EC_{50}, V_{max} = the maximum observable efflux (set to 100 %) and *n* is the Hill coefficient.

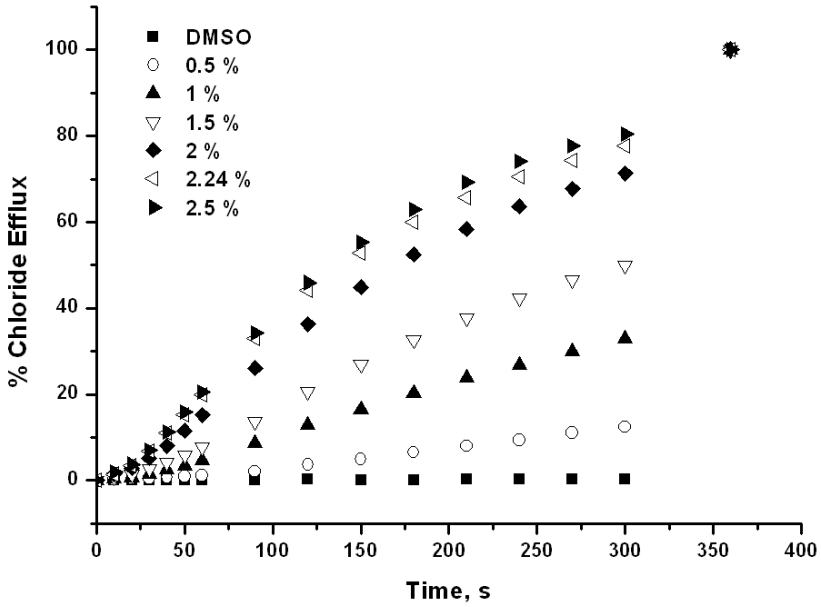

Figure S25 Chloride efflux mediated by various concentrations (mol% w.r.t. lipid) of receptor **10** from unilamellar POPC vesicles loaded with 489 mM NaCl buffered to pH 7.2 with 5 mM sodium phosphate salts. The vesicles were suspended in 489 mM $NaNO_3$ buffered to pH 7.2 with 5 mM sodium phosphate salts. At the end of the experiment the vesicles were lysed by the addition of detergent to calibrate 100 % chloride efflux. Each point represents the average of 3 trials.

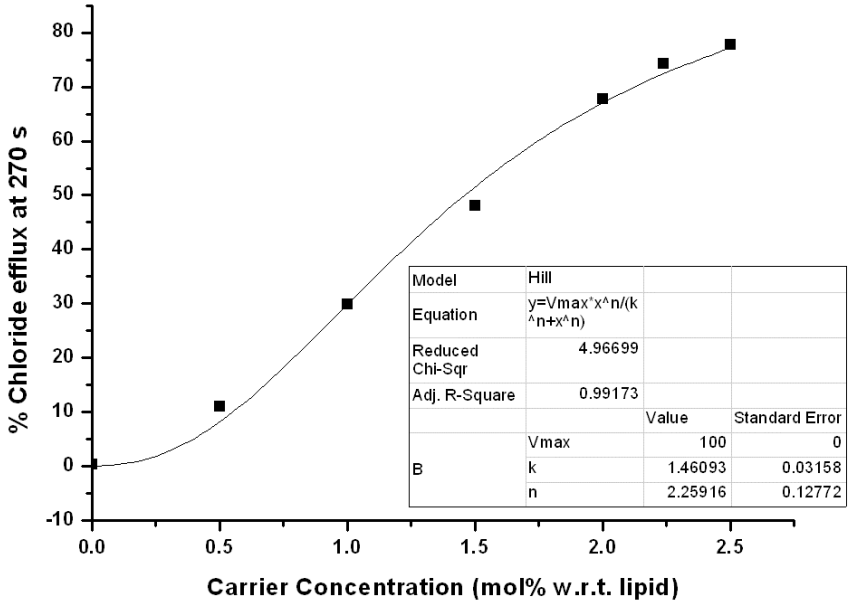

Figure S26 Hill plot for the Cl^-/NO_3^- antiport mediated by receptor **10** after 270 s, where k = EC_{50}, V_{max} = the maximum observable efflux (set to 100 %) and *n* is the Hill coefficient.

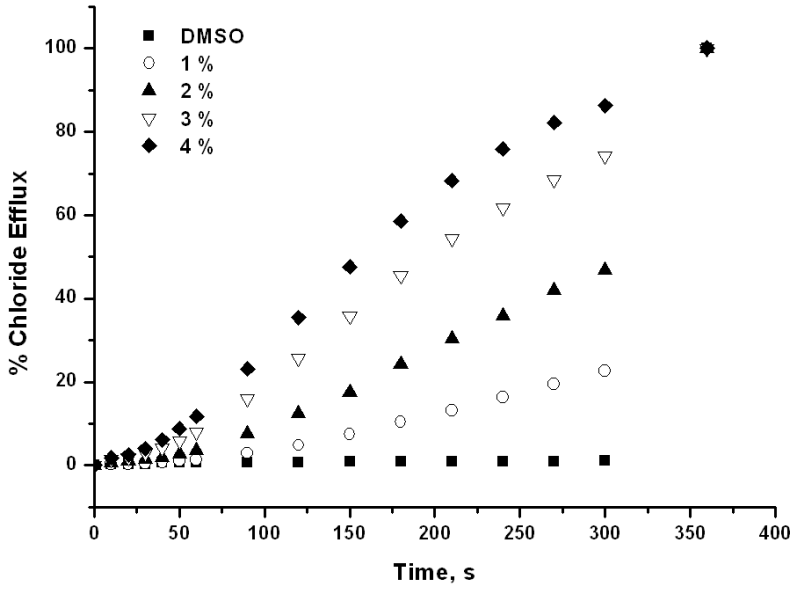

Figure S27 Chloride efflux mediated by various concentrations (mol% w.r.t. lipid) of receptor **11** from unilamellar POPC vesicles loaded with 489 mM NaCl buffered to pH 7.2 with 5 mM sodium phosphate salts. The vesicles were suspended in 489 mM $NaNO_3$ buffered to pH 7.2 with 5 mM sodium phosphate salts. At the end of the experiment the vesicles were lysed by the addition of detergent to calibrate 100 % chloride efflux. Each point represents the average of 3 trials.

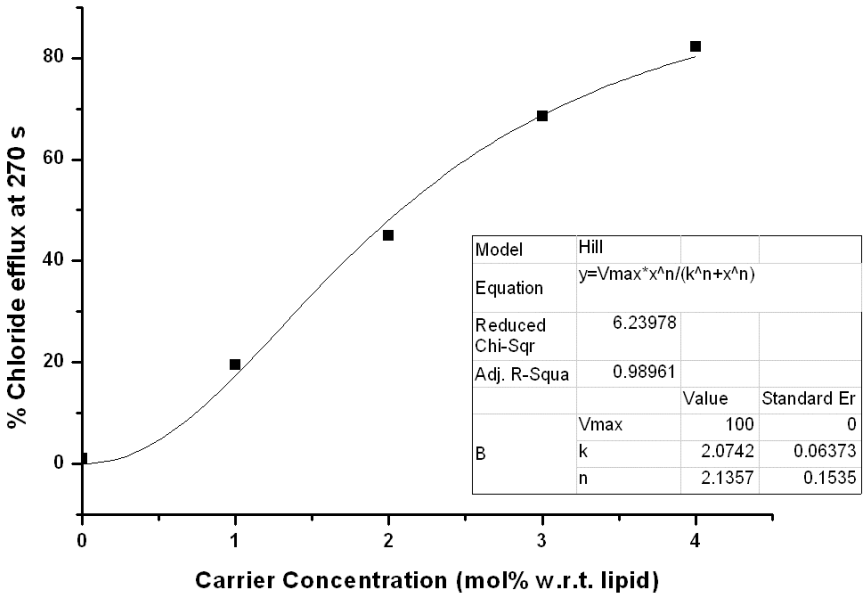

Figure S28 Hill plot for the Cl^-/NO_3^- antiport mediated by receptor **11** after 270 s, where k = EC_{50}, V_{max} = the maximum observable efflux (set to 100 %) and *n* is the Hill coefficient.

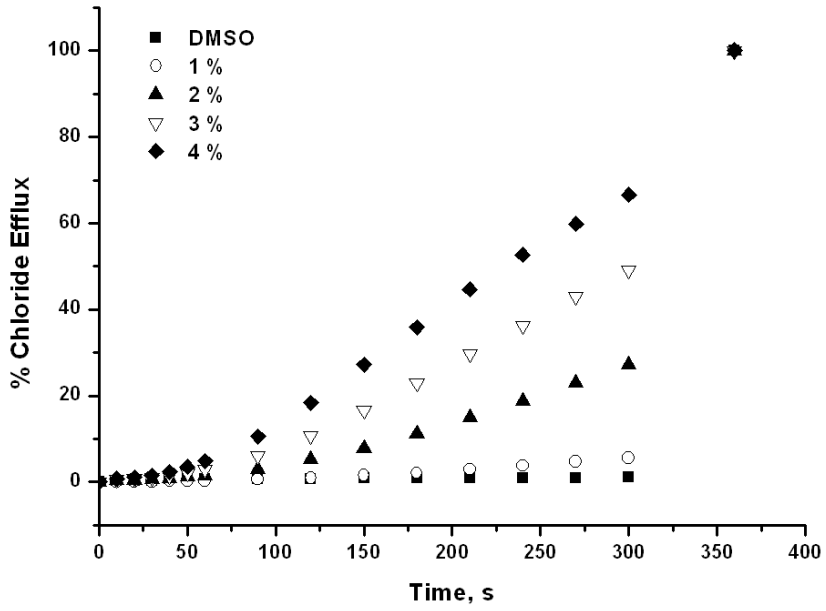

Figure S29 Chloride efflux mediated by various concentrations (mol% w.r.t. lipid) of receptor **12** from unilamellar POPC vesicles loaded with 489 mM NaCl buffered to pH 7.2 with 5 mM sodium phosphate salts. The vesicles were suspended in 489 mM $NaNO_3$ buffered to pH 7.2 with 5 mM sodium phosphate salts. At the end of the experiment the vesicles were lysed by the addition of detergent to calibrate 100 % chloride efflux. Each point represents the average of 3 trials.

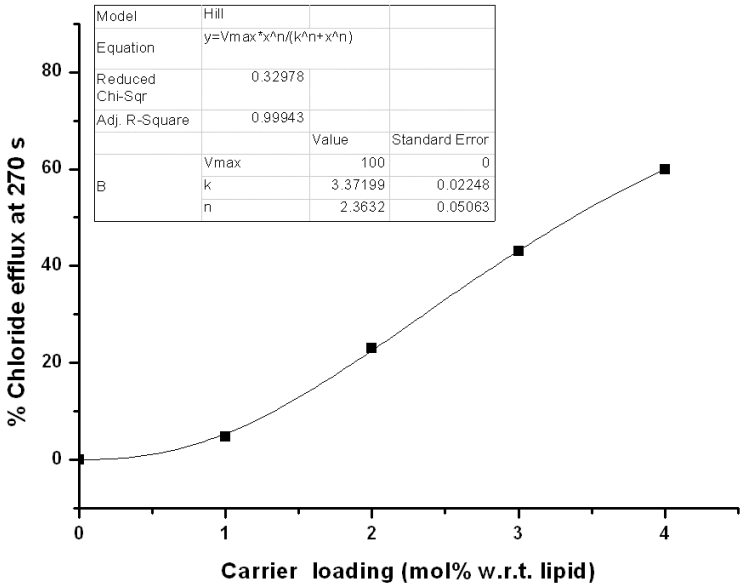

Figure S30 Hill plot for the Cl^-/NO_3^- antiport mediated by receptor **12** after 270 s, where k = EC_{50}, V_{max} = the maximum observable efflux (set to 100 %) and *n* is the Hill coefficient.

Cholesterol assays

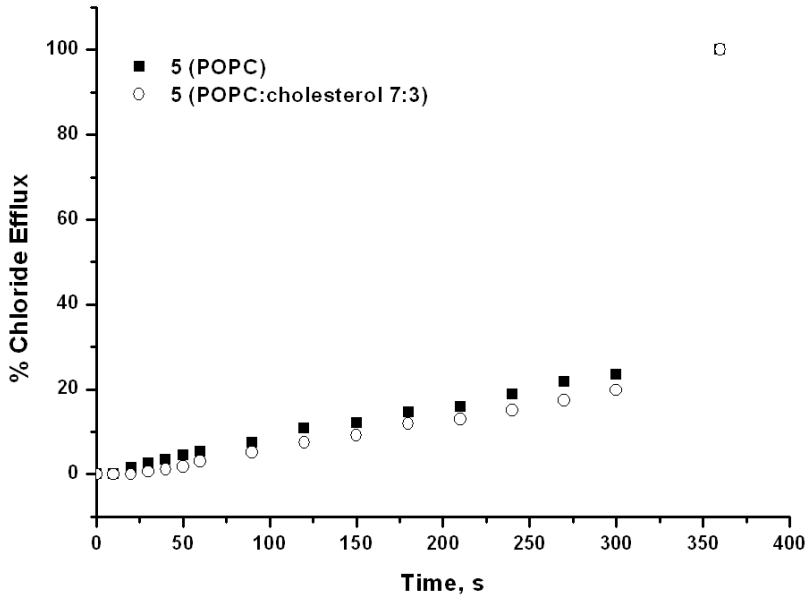

Figure S31 Chloride efflux mediated by receptor **5 (**2 mol% w.r.t. lipid) from unilamellar vesicles composed of POPC or POPC:cholesterol (7:3) loaded with 489 mM NaCl buffered to pH 7.2 with 5 mM sodium phosphate salts. The vesicles were suspended in 489 mM $NaNO_3$ buffered to pH 7.2 with 5 mM sodium phosphate salts. At the end of the experiment the vesicles were lysed by the addition of detergent to calibrate 100 % chloride efflux. Each point represents the average of 3 trials.

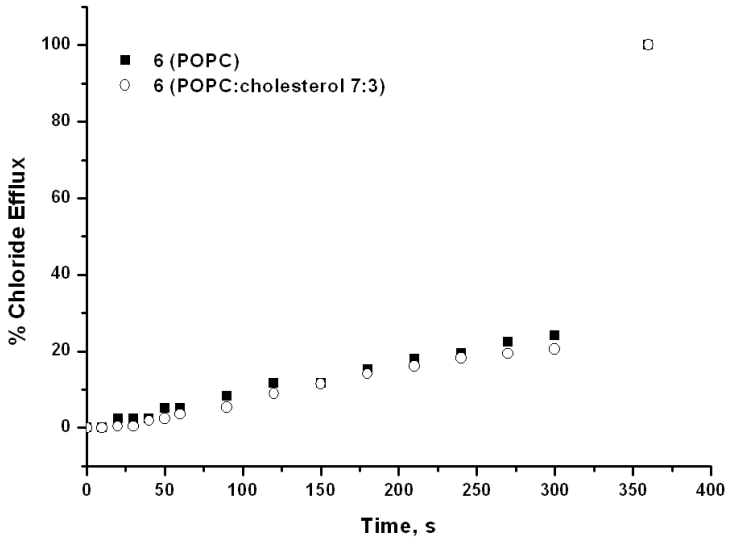

Figure S32 Chloride efflux mediated by receptor **6 (**2 mol% w.r.t. lipid) from unilamellar vesicles composed of POPC or POPC:cholesterol (7:3) loaded with 489 mM NaCl buffered to pH 7.2 with 5 mM sodium phosphate salts. The vesicles were suspended in 489 mM $NaNO_3$ buffered to pH 7.2 with 5 mM sodium phosphate salts. At the end of the experiment the vesicles were lysed by the addition of detergent to calibrate 100 % chloride efflux. Each point represents the average of 3 trials.

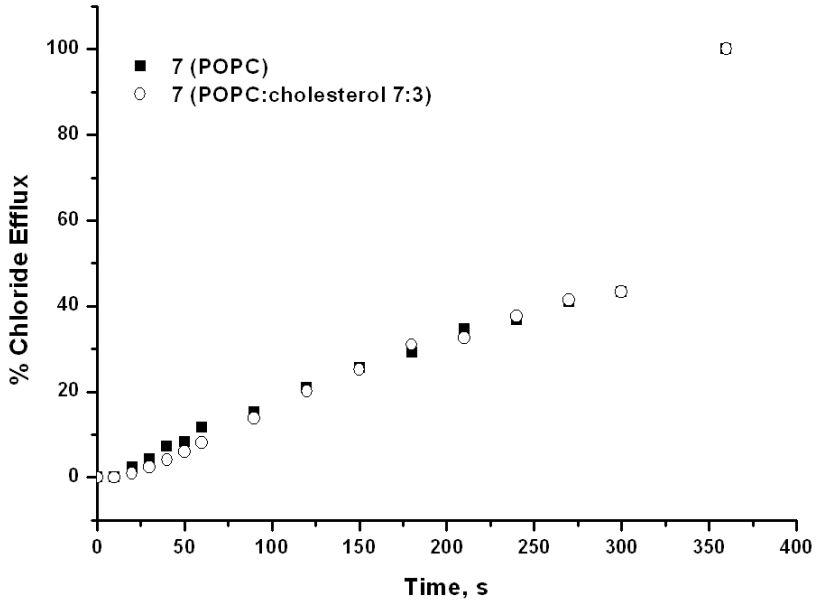

Figure S33 Chloride efflux mediated by receptor **7 (**2 mol% w.r.t. lipid) from unilamellar vesicles composed of POPC or POPC:cholesterol (7:3) loaded with 489 mM NaCl buffered to pH 7.2 with 5 mM sodium phosphate salts. The vesicles were suspended in 489 mM $NaNO_3$ buffered to pH 7.2 with 5 mM sodium phosphate salts. At the end of the experiment the vesicles were lysed by the addition of detergent to calibrate 100 % chloride efflux. Each point represents the average of 3 trials.

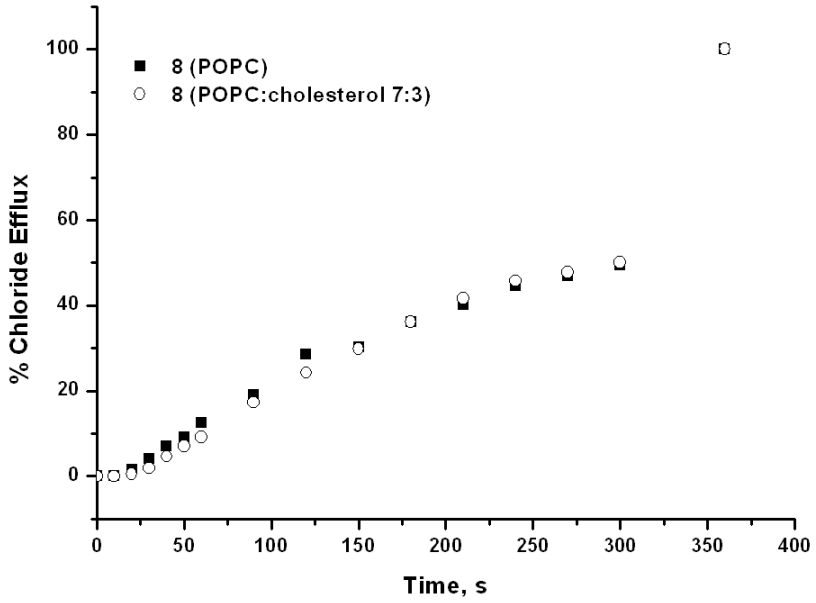

Figure S34 Chloride efflux mediated by receptor **8 (**2 mol% w.r.t. lipid) from unilamellar vesicles composed of POPC or POPC:cholesterol (7:3) loaded with 489 mM NaCl buffered to pH 7.2 with 5 mM sodium phosphate salts. The vesicles were suspended in 489 mM $NaNO_3$ buffered to pH 7.2 with 5 mM sodium phosphate salts. At the end of the experiment the vesicles were lysed by the addition of detergent to calibrate 100 % chloride efflux. Each point represents the average of 3 trials.

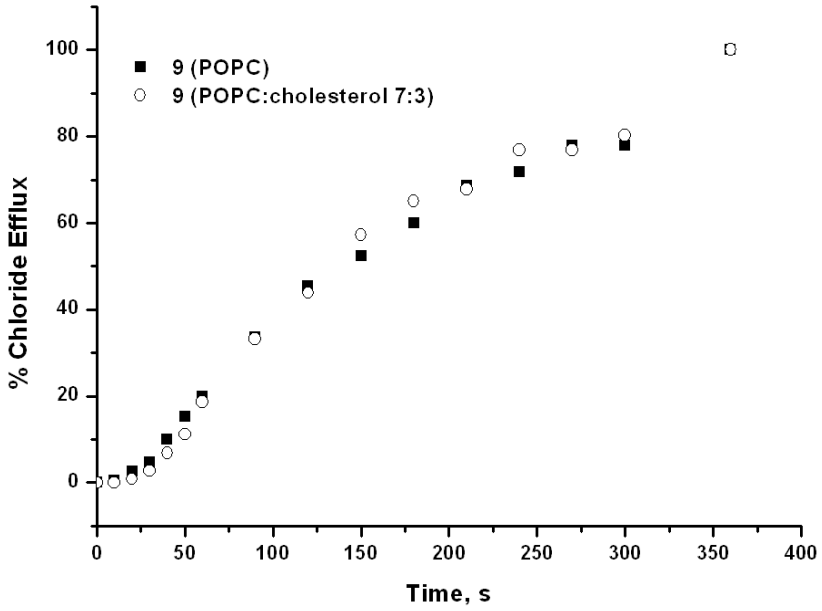

Figure S35 Chloride efflux mediated by receptor **9 (**2 mol% w.r.t. lipid) from unilamellar vesicles composed of POPC or POPC:cholesterol (7:3) loaded with 489 mM NaCl buffered to pH 7.2 with 5 mM sodium phosphate salts. The vesicles were suspended in 489 mM $NaNO_3$ buffered to pH 7.2 with 5 mM sodium phosphate salts. At the end of the experiment the vesicles were lysed by the addition of detergent to calibrate 100 % chloride efflux. Each point represents the average of 3 trials.

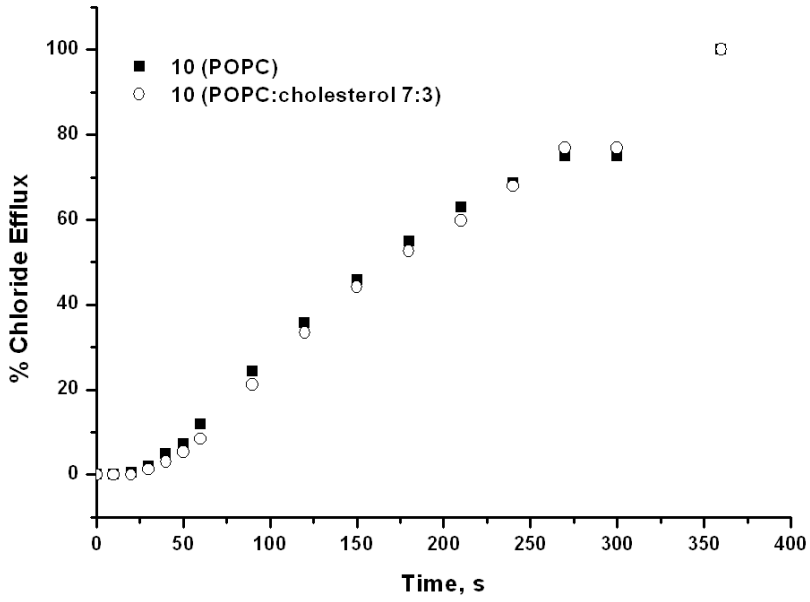

Figure S36 Chloride efflux mediated by receptor **10 (**2 mol% w.r.t. lipid) from unilamellar vesicles composed of POPC or POPC:cholesterol (7:3) loaded with 489 mM NaCl buffered to pH 7.2 with 5 mM sodium phosphate salts. The vesicles were suspended in 489 mM $NaNO_3$ buffered to pH 7.2 with 5 mM sodium phosphate salts. At the end of the experiment the vesicles were lysed by the addition of detergent to calibrate 100 % chloride efflux. Each point represents the average of 3 trials.

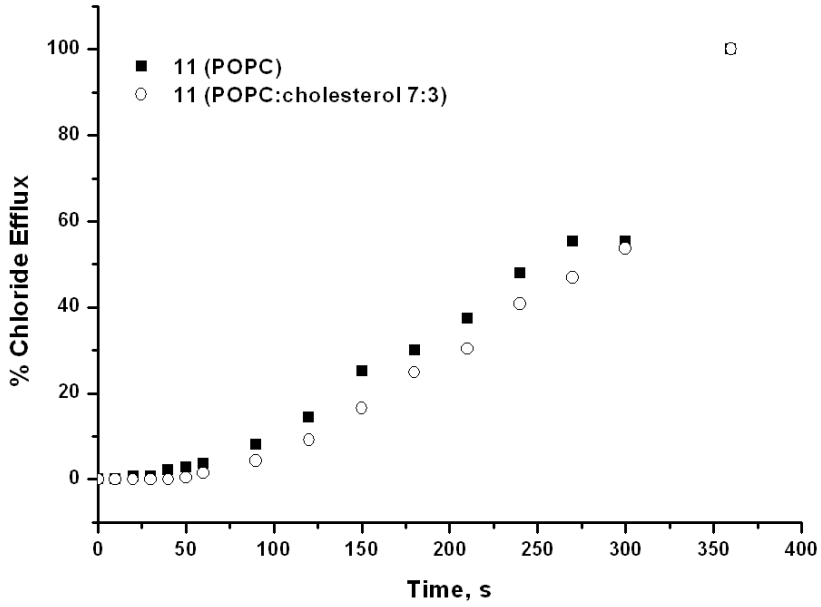

Figure S37 Chloride efflux mediated by receptor **11 (**2 mol% w.r.t. lipid) from unilamellar vesicles composed of POPC or POPC:cholesterol (7:3) loaded with 489 mM NaCl buffered to pH 7.2 with 5 mM sodium phosphate salts. The vesicles were suspended in 489 mM $NaNO_3$ buffered to pH 7.2 with 5 mM sodium phosphate salts. At the end of the experiment the vesicles were lysed by the addition of detergent to calibrate 100 % chloride efflux. Each point represents the average of 3 trials.

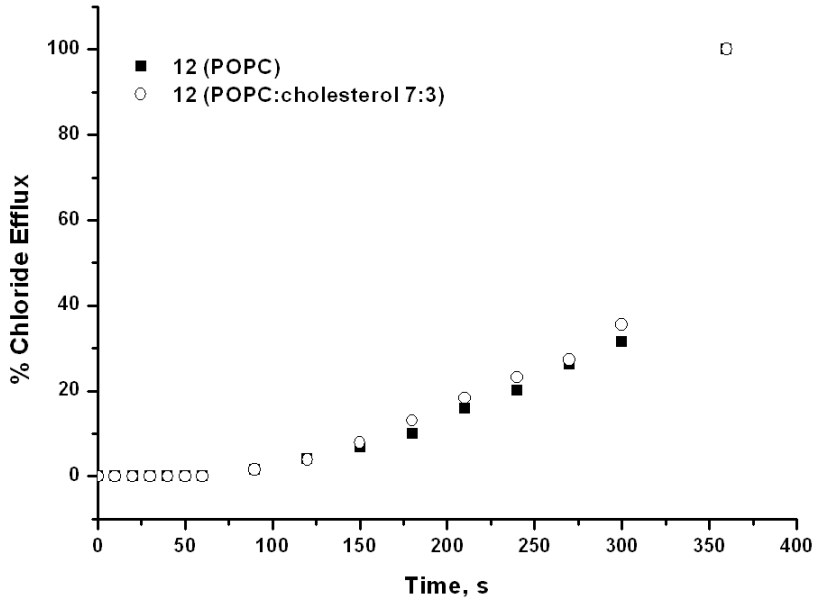

Figure S38 Chloride efflux mediated by receptor **12 (**2 mol% w.r.t. lipid) from unilamellar vesicles composed of POPC or POPC:cholesterol (7:3) loaded with 489 mM NaCl buffered to pH 7.2 with 5 mM sodium phosphate salts. The vesicles were suspended in 489 mM $NaNO_3$ buffered to pH 7.2 with 5 mM sodium phosphate salts. At the end of the experiment the vesicles were lysed by the addition of detergent to calibrate 100 % chloride efflux. Each point represents the average of 3 trials.

Variation of bilayer thickness

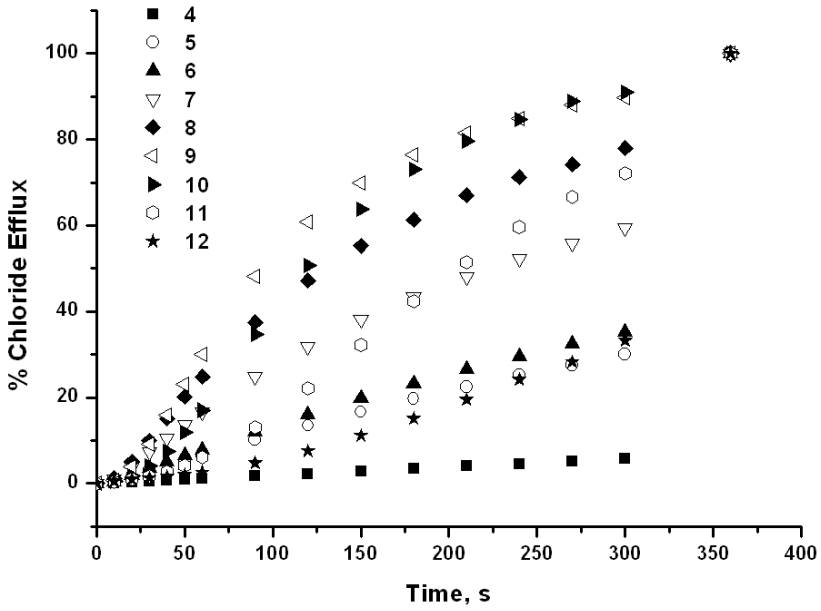

Figure S39 Chloride efflux mediated by receptors **4-12** (2 mol% w.r.t. lipid) from unilamellar vesicles composed of C_{16}PC loaded with 489 mM NaCl buffered to pH 7.2 with 5 mM sodium phosphate salts. The vesicles were suspended in 489 mM $NaNO_3$ buffered to pH 7.2 with 5 mM sodium phosphate salts. At the end of the experiment the vesicles were lysed by the addition of detergent to calibrate 100 % chloride efflux. Each point represents the average of 3 trials.

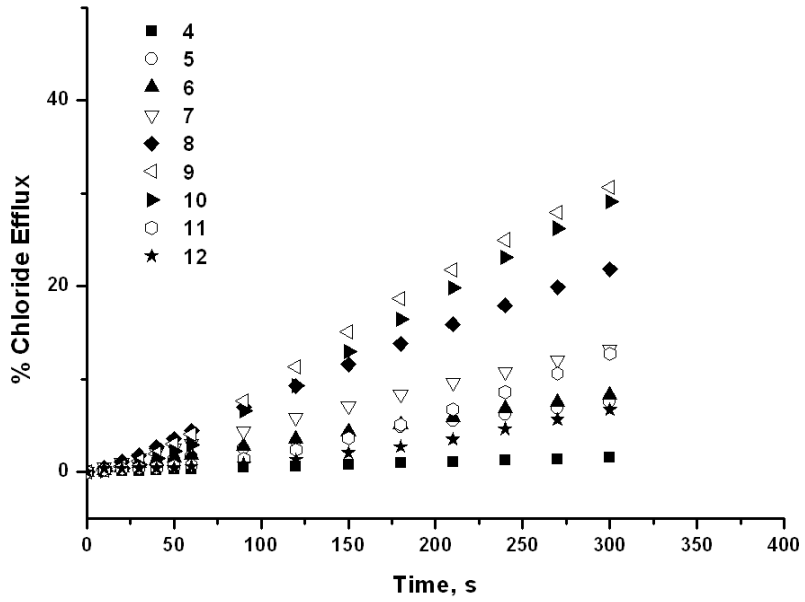

Figure S40 Chloride efflux mediated by receptors **4-12** (2 mol% w.r.t. lipid) from unilamellar vesicles composed of C_{18}PC loaded with 489 mM NaCl buffered to pH 7.2 with 5 mM sodium phosphate salts. The vesicles were suspended in 489 mM $NaNO_3$ buffered to pH 7.2 with 5 mM sodium phosphate salts. At the end of the experiment the vesicles were lysed by the addition of detergent to calibrate 100 % chloride efflux. Each point represents the average of 3 trials.

NMR titrations

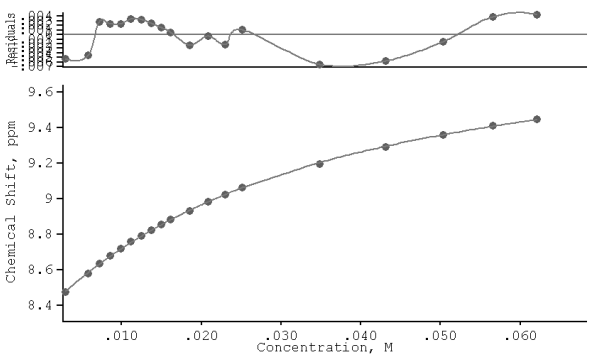

Figure S41 Binding curve from the ^{1}H NMR titration of receptor **4** with tetrabutylammonium chloride (TBACl) in DMSO-d_5/ H_2O 0.5 % following the urea NH resonance at ~8.3 ppm. The data was fitted to a 1:1 biding model using WinEQNMR 2. K_a = 37 M^{-1} (0.857).

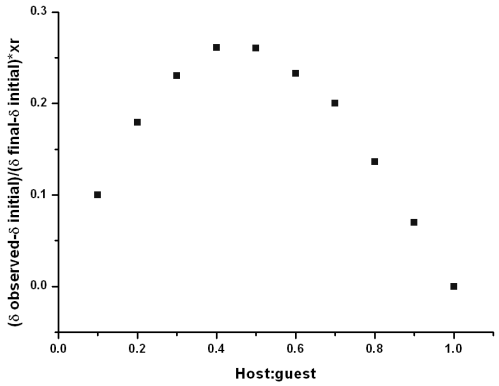

Figure S42 Job plot analysis for the interaction of receptor **4** with TBACl following the urea NH resonance at ~8.3 ppm.

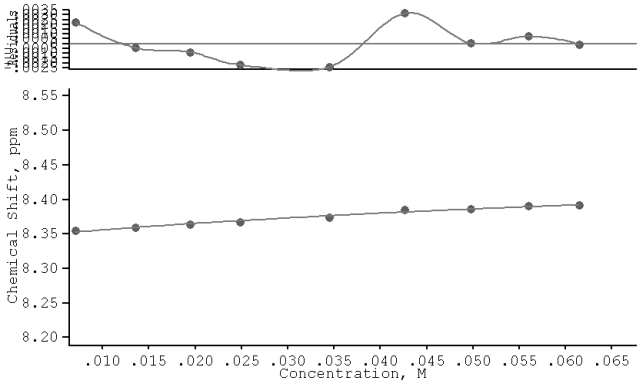

Figure S43 Binding curve from the ^{1}H NMR titration of receptor **4** with tetrabutylammonium nitrate ($TBANO_3$) in DMSO-d_5/ H_2O 0.5 % following the urea NH resonance at ~8.3 ppm. The data was fitted to a 1:1 binding model using WinEQNMR 2. $K_a < 10$ M^{-1}.

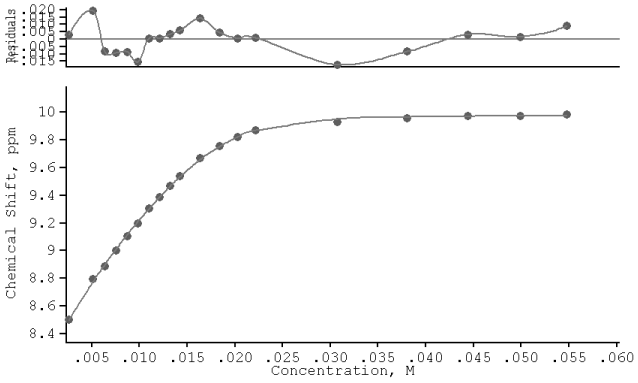

Figure S44 Binding curve from the ^{1}H NMR titration of receptor **4** with tetraethylammonium bicarbonate ($TEAHCO_3$) in DMSO-d_5/ H_2O 0.5 % following the urea NH resonance at ~8.3 ppm. The data was fitted to a 1:2 binding model using WinEQNMR 2. $b_1 = K_1 = 802\ M^{-1}$ (105.4), $b_2 = 660442\ M^{-2}$ (20610).

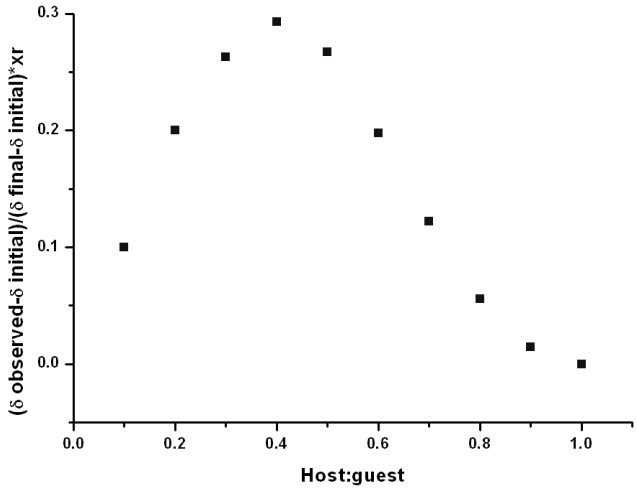

Figure S45 Job plot analysis for the interaction of receptor **4** with $TEAHCO_3$ following the urea NH resonance at ~8.3 ppm.

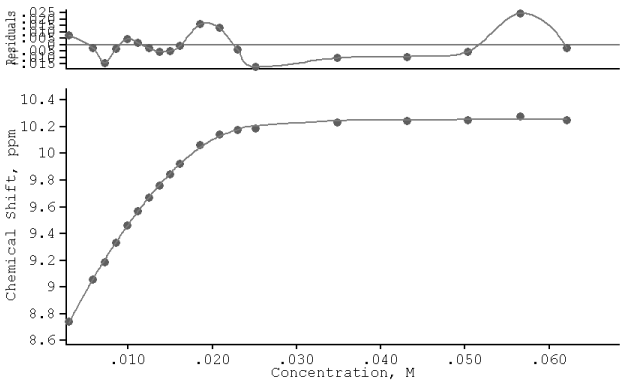

Figure S46 Binding curve from the ^{1}H NMR titration of receptor **4** with tetrabutylammonium dihydrogen phosphate ($TBAH_2PO_4$) in DMSO-d_5/ H_2O 0.5 % following the urea NH resonance at ~8.3 ppm. The data was fitted to a 1:2 binding model using WinEQNMR 2. $b_1 = K_1 = 722$ M^{-1} (105.2), $b_2 = 752348$ M^{-2} (31800).

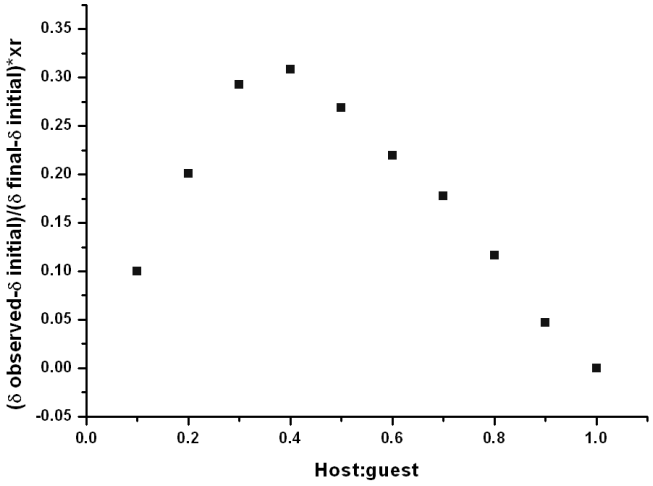

Figure S47 Job plot analysis for the interaction of receptor **4** with $TBAH_2PO_4$ following the urea NH resonance at ~8.3 ppm.

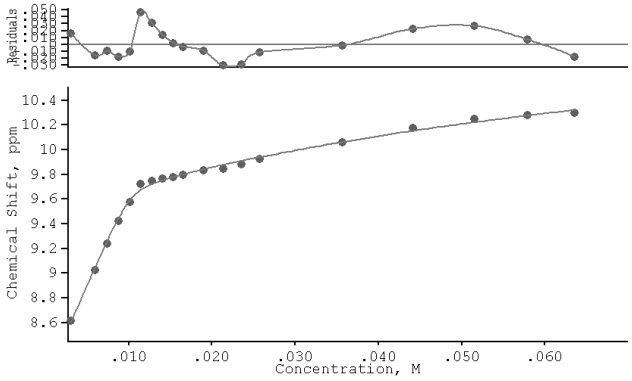

Figure S48 Binding curve from the ^{1}H NMR titration of receptor **4** with tetrabutylammonium sulfate (TBA_2SO_4) in DMSO-d_5/ H_2O 0.5 % following the urea NH resonance at ~8.3 ppm. The data was fitted to a 1:2 binding model using WinEQNMR 2. $b_1 = K_1 > 10^4$ M^{-1}, $b_2 = 178800$ M^{-2} (40880).

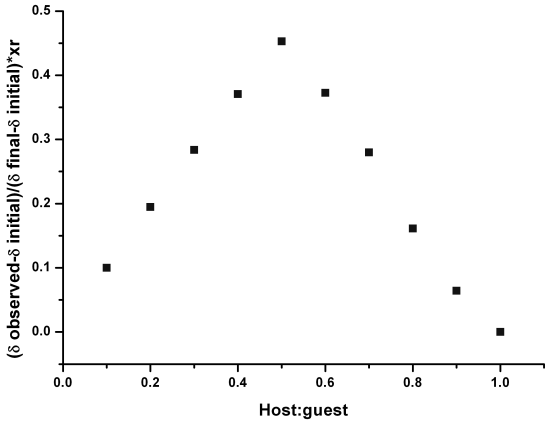

Figure S49 Job plot analysis for the interaction of receptor **4** with TBA_2SO_4 following the urea NH resonance at ~8.3 ppm.

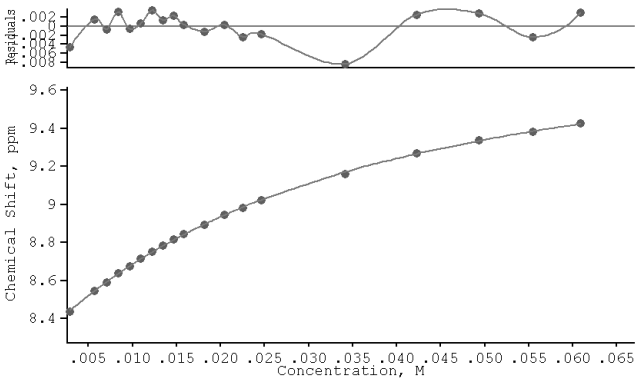

Figure S50 Binding curve from the ^{1}H NMR titration of receptor **5** with TBACl in DMSO-d_5/ H_2O 0.5 % following the urea NH resonance at ~8.3 ppm. The data was fitted to a 1:1 biding model using WinEQNMR 2. K_a = 35 M^{-1} (0.6944).

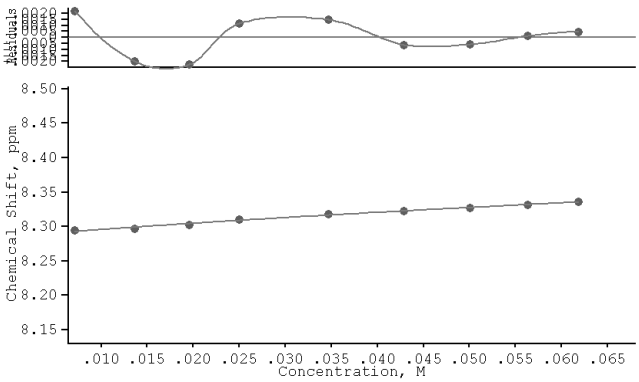

Figure S51 Binding curve from the ^{1}H NMR titration of receptor **5** with $TBANO_3$ in DMSO-d_5/ H_2O 0.5 % following the urea NH resonance at ~8.3 ppm. The data was fitted to a 1:1 biding model using WinEQNMR 2. K_a < 10 M^{-1}.

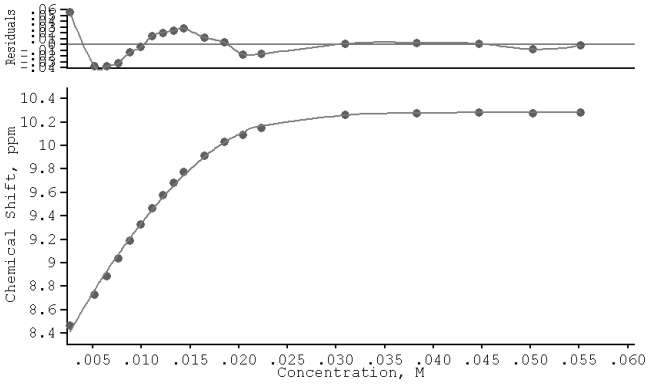

Figure S52 Binding curve from the ^{1}H NMR titration of receptor **5** with $TEAHCO_3$ in DMSO-d_5/ H_2O 0.5 % following the urea NH resonance at ~8.3 ppm. The data was fitted to a 1:2 binding model using WinEQNMR 2. $b_1 = K_1 = 1178$ M^{-1} (304.4), $b_2 = 1067700$ M^{-2} (45340).

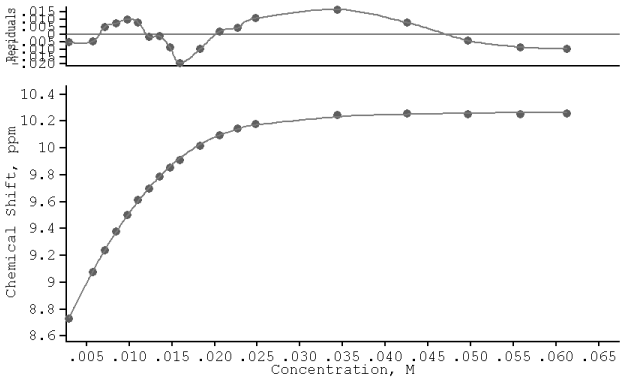

Figure S53 Binding curve from the ^{1}H NMR titration of receptor **5** with $TBAH_2PO_4$ in DMSO-d_5/ H_2O 0.5 % following the urea NH resonance at ~8.3 ppm. The data was fitted to a 1:2 binding model using WinEQNMR 2. $b_1 = K_1 = 1542$ M^{-1} (131.5), $b_2 = 702727$ M^{-2} (19250).

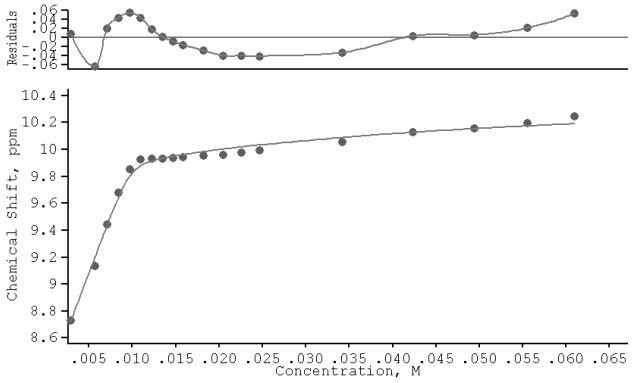

Figure S54 Binding curve from the ^{1}H NMR titration of receptor **5** with TBA_2SO_4 in DMSO-d_5/ H_2O 0.5 % following the urea NH resonance at ~8.3 ppm. The data was fitted to a 1:2 binding model using WinEQNMR 2. $b_1 = K_1 > 10^4$ M^{-1}, $b_2 = 567017$ M^{-2} (99590).

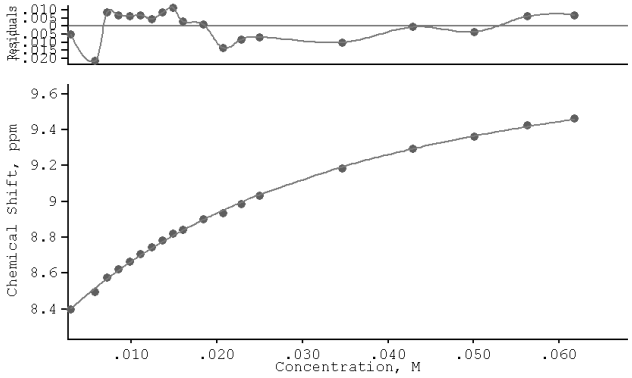

Figure S55 Binding curve from the ^{1}H NMR titration of receptor **6** with TBACl in DMSO-d_5/ H_2O 0.5 % following the urea NH resonance at ~8.3 ppm. The data was fitted to a 1:1 biding model using WinEQNMR 2. $K_a = 37$ M^{-1} (1.953).

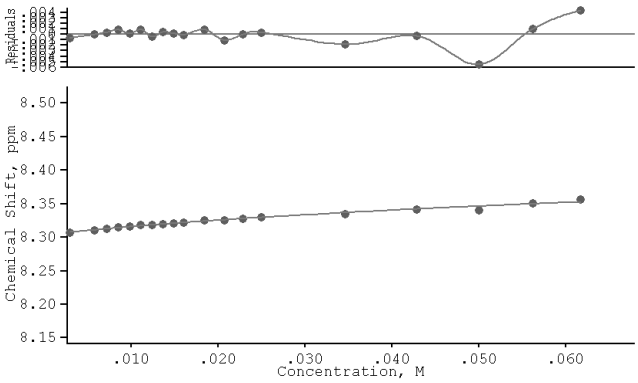

Figure S56 Binding curve from the ^{1}H NMR titration of receptor **6** with $TBANO_3$ in DMSO-d_5/ H_2O 0.5 % following the urea NH resonance at ~8.3 ppm. The data was fitted to a 1:1 biding model using WinEQNMR 2. $K_a < 10$ M^{-1}.

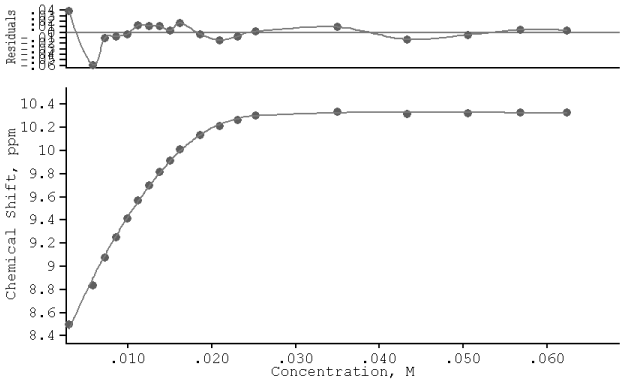

Figure S57 Binding curve from the ^{1}H NMR titration of receptor **6** with $TEAHCO_3$ in DMSO-d_5/ H_2O 0.5 % following the urea NH resonance at ~8.3 ppm. The data was fitted to a 1:2 binding model using WinEQNMR 2. $b_1 = K_1 = 8131$ M^{-1} (176.2), $b_2 = 862682$ M^{-2} (45590).

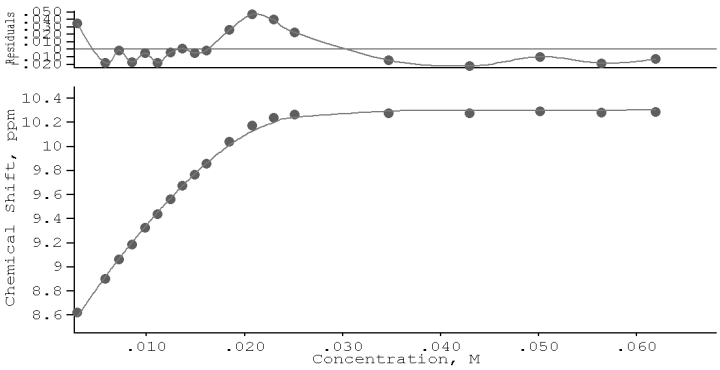

Figure S58 Binding curve from the ^{1}H NMR titration of receptor **6** with $TBAH_2PO_4$ in DMSO-d_5/ H_2O 0.5 % following the urea NH resonance at ~8.3 ppm. The data was fitted to a 1:2 binding model using WinEQNMR 2. $b_1 = K_1$ = 386 M^{-1} (108.2), b_2 = 627030 M^{-2} (80940).

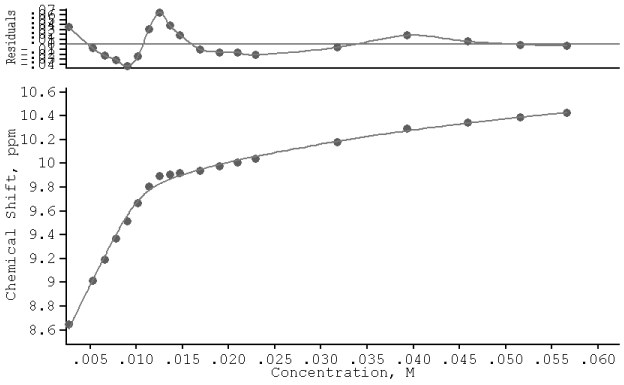

Figure S59 Binding curve from the ^{1}H NMR titration of receptor **6** with TBA_2SO_4 in DMSO-d_5/ H_2O 0.5 % following the urea NH resonance at ~8.3 ppm. The data was fitted to a 1:2 binding model using WinEQNMR 2. $b_1 = K_1$ = 9768 M^{-1} (1932), b_2 = 192435 M^{-2} (48660).

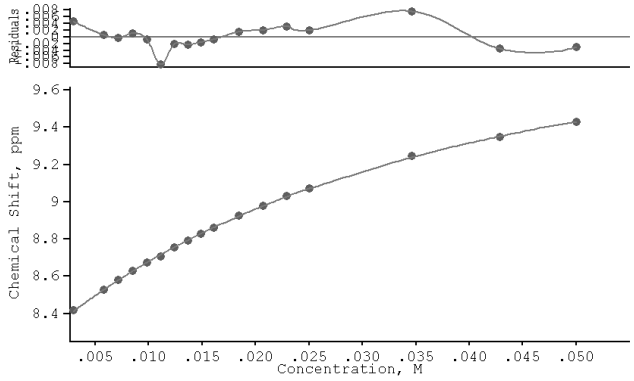

Figure S60 Binding curve from the ^{1}H NMR titration of receptor **7** with TBACl in DMSO-d_5/ H_2O 0.5 % following the urea NH resonance at ~8.3 ppm. The data was fitted to a 1:1 biding model using WinEQNMR 2. K_a = 32 M^{-1} (0.8869).

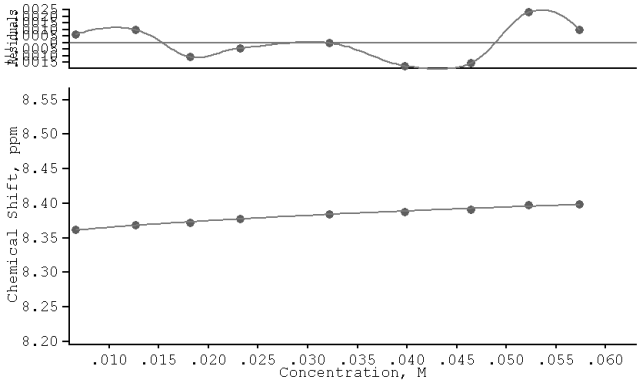

Figure S61 Binding curve from the ^{1}H NMR titration of receptor **7** with $TBANO_3$ in DMSO-d_5/ H_2O 0.5 % following the urea NH resonance at ~8.3 ppm. The data was fitted to a 1:1 biding model using WinEQNMR 2. K_a < 10 M^{-1}.

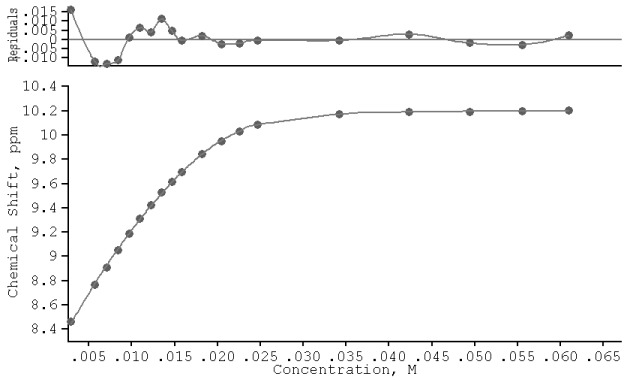

Figure S62 Binding curve from the ^{1}H NMR titration of receptor **7** with $TEAHCO_3$ in DMSO-d_5/ H_2O 0.5 % following the urea NH resonance at ~8.3 ppm. The data was fitted to a 1:2 binding model using WinEQNMR 2. $b_1 = K_1 = 584$ M^{-1} (61.44), $b_2 = 465949$ M^{-2} (790).

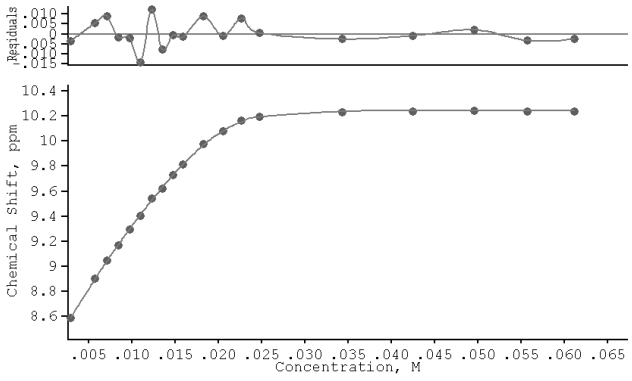

Figure S63 Binding curve from the ^{1}H NMR titration of receptor **7** with $TBAH_2PO_4$ in DMSO-d_5/ H_2O 0.5 % following the urea NH resonance at ~8.3 ppm. The data was fitted to a 1:2 binding model using WinEQNMR 2. $b_1 = K_1 = 341$ M^{-1} (66.77), $b_2 = 789322$ M^{-2} (17010).

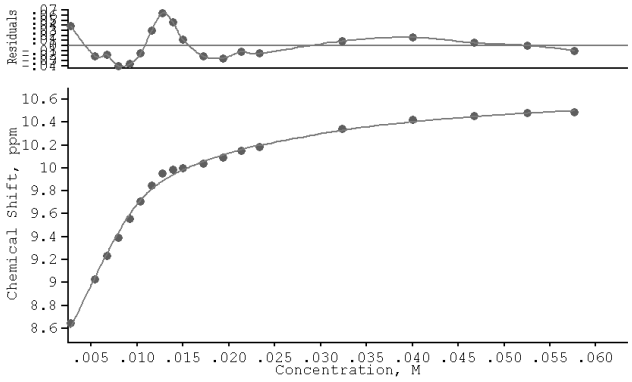

Figure S64 Binding curve from the ^{1}H NMR titration of receptor **7** with TBA_2SO_4 in DMSO-d_5/ H_2O 0.5 % following the urea NH resonance at ~8.3 ppm. The data was fitted to a 1:2 binding model using WinEQNMR 2. $b_1 = K_1 = 7170$ M^{-1} (1216), $b_2 = 512992$ M^{-2} (59230).

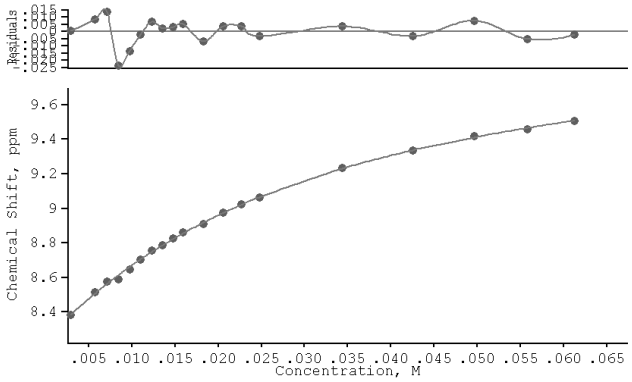

Figure S65 Binding curve from the ^{1}H NMR titration of receptor **8** with TBACl in DMSO-d_5/ H_2O 0.5 % following the urea NH resonance at ~8.3 ppm. The data was fitted to a 1:1 biding model using WinEQNMR 2. $K_a = 39$ M^{-1} (1.806).

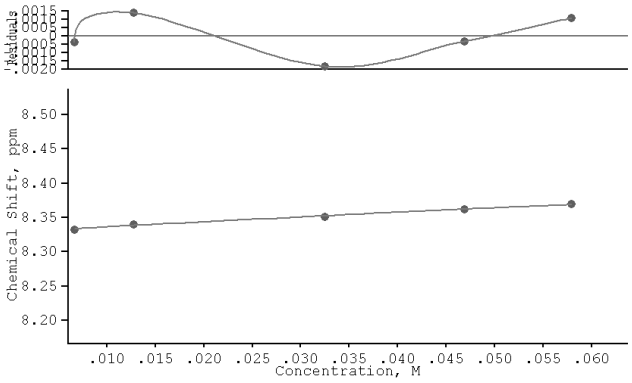

Figure S66 Binding curve from the ^{1}H NMR titration of receptor **8** with $TBANO_3$ in DMSO-d_5/ H_2O 0.5 % following the urea NH resonance at ~8.3 ppm. The data was fitted to a 1:1 biding model using WinEQNMR 2. $K_a < 10$ M^{-1}.

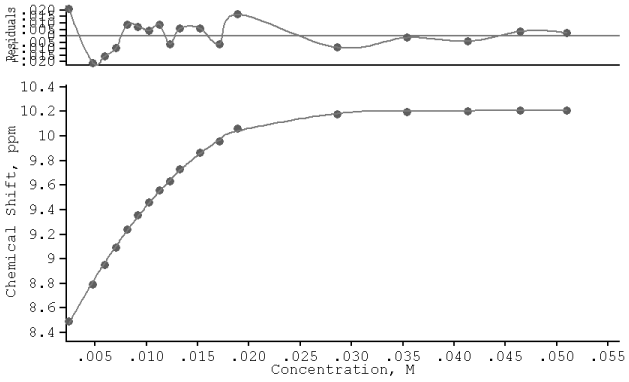

Figure S67 Binding curve from the ^{1}H NMR titration of receptor **8** with $TEAHCO_3$ in DMSO-d_5/ H_2O 0.5 % following the urea NH resonance at ~8.3 ppm. The data was fitted to a 1:2 binding model using WinEQNMR 2. $b_1 = K_1 = 1101$ M^{-1} (169), $b_2 = 837798$ M^{-2} (35830).

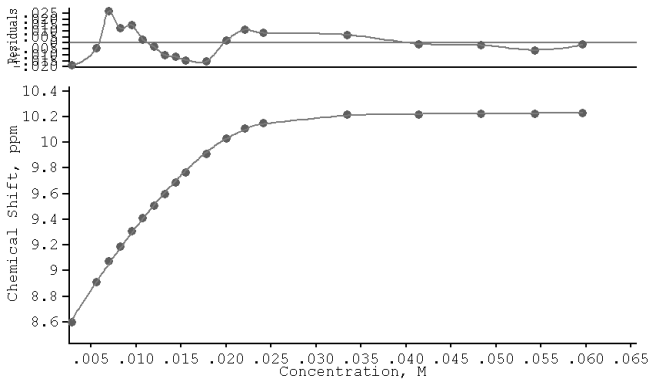

Figure S68 Binding curve from the ^{1}H NMR titration of receptor **8** with $TBAH_2PO_4$ in DMSO-d_5/ H_2O 0.5 % following the urea NH resonance at ~8.3 ppm. The data was fitted to a 1:2 binding model using WinEQNMR 2. $b_1 = K_1$ = 420 M^{-1} (99.67), b_2 = 542492 M^{-2} (27860).

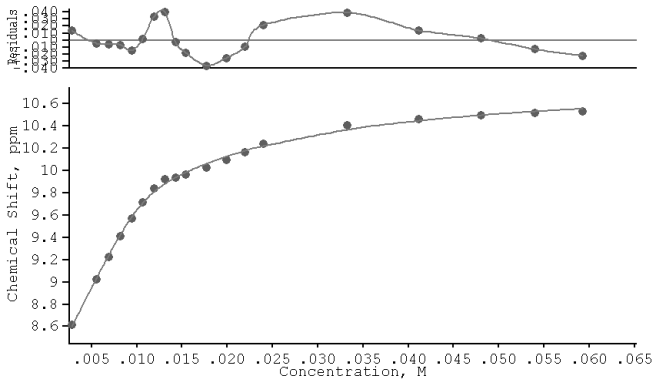

Figure S69 Binding curve from the ^{1}H NMR titration of receptor **8** with TBA_2SO_4 in DMSO-d_5/ H_2O 0.5 % following the urea NH resonance at ~8.3 ppm. The data was fitted to a 1:2 binding model using WinEQNMR 2. $b_1 = K_1$ = 8560 M^{-1} (1125), b_2 = 623547 M^{-2} (36340).

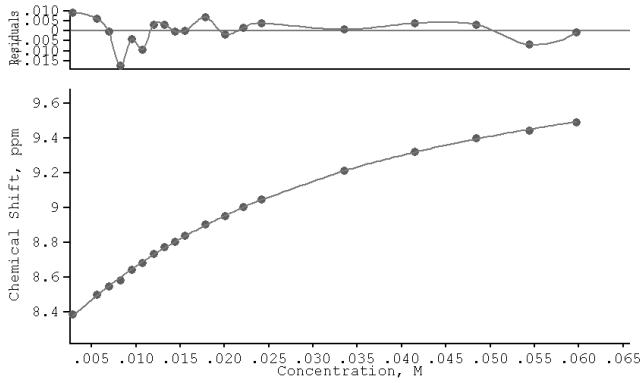

Figure S70 Binding curve from the ^{1}H NMR titration of receptor **9** with TBACl in DMSO-d_5/ H_2O 0.5 % following the urea NH resonance at ~8.3 ppm. The data was fitted to a 1:1 biding model using WinEQNMR 2. K_a = 38 M^{-1} (1.309).

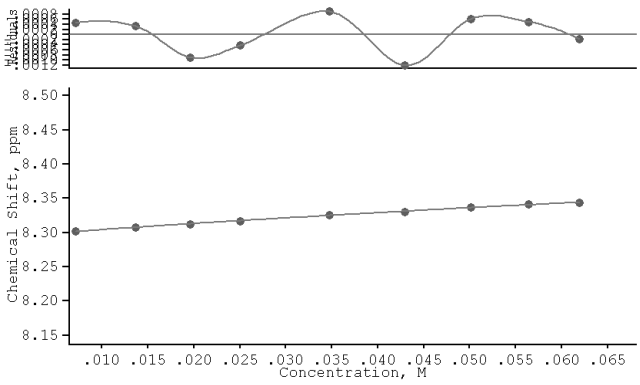

Figure S71 Binding curve from the ^{1}H NMR titration of receptor **9** with $TBANO_3$ in DMSO-d_5/ H_2O 0.5 % following the urea NH resonance at ~8.3 ppm. The data was fitted to a 1:1 biding model using WinEQNMR 2. K_a < 10 M^{-1}.

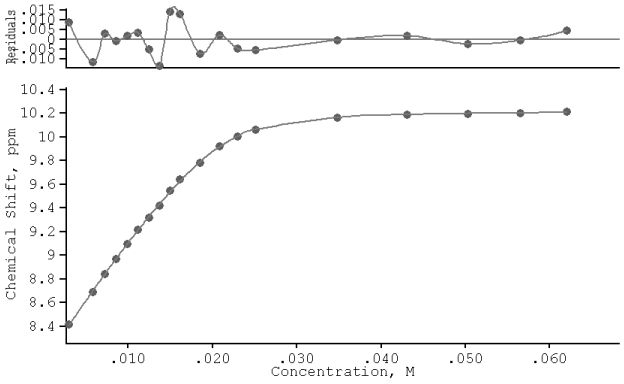

Figure S72 Binding curve from the ^{1}H NMR titration of receptor **9** with $TEAHCO_3$ in DMSO-d_5/ H_2O 0.5 % following the urea NH resonance at ~8.3 ppm. The data was fitted to a 1:2 binding model using WinEQNMR 2. $b_1 = K_1 = 560$ M^{-1} (60.5), $b_2 = 583357$ M^{-2} (21680).

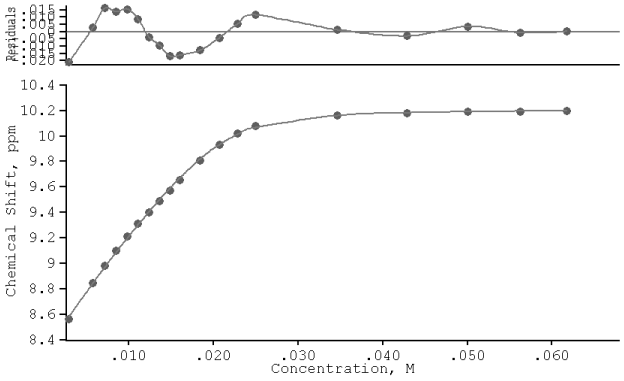

Figure S73 Binding curve from the ^{1}H NMR titration of receptor **9** with $TBAH_2PO_4$ in DMSO-d_5/ H_2O 0.5 % following the urea NH resonance at ~8.3 ppm. The data was fitted to a 1:2 binding model using WinEQNMR 2. $b_1 = K_1 = 572$ M^{-1} (103.6), $b_2 = 585002$ M^{-2} (32430).

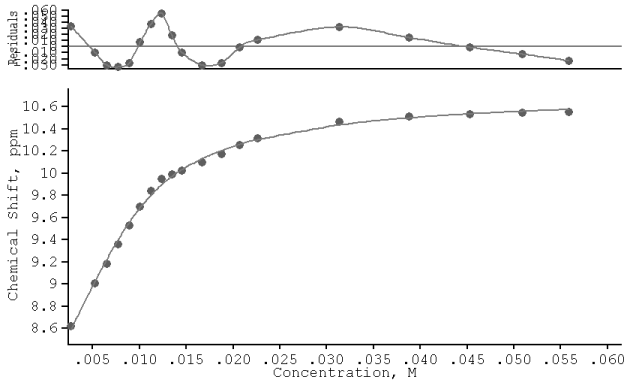

Figure S74 Binding curve from the ^{1}H NMR titration of receptor **9** with TBA_2SO_4 in DMSO-d_5/ H_2O 0.5 % following the urea NH resonance at ~8.3 ppm. The data was fitted to a 1:2 binding model using WinEQNMR 2. $b_1 = K_1 = 3280$ M^{-1} (643.9), $b_2 = 360871$ M^{-2} (45020).

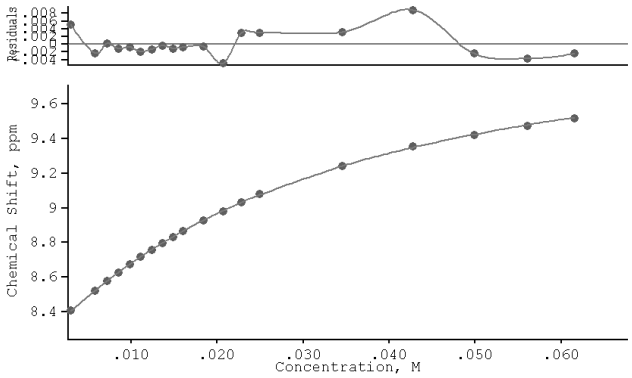

Figure S75 Binding curve from the ^{1}H NMR titration of receptor **10** with TBACl in DMSO-d_5/ H_2O 0.5 % following the urea NH resonance at ~8.3 ppm. The data was fitted to a 1:1 biding model using WinEQNMR 2. $K_a = 37$ M^{-1} (0.6931).

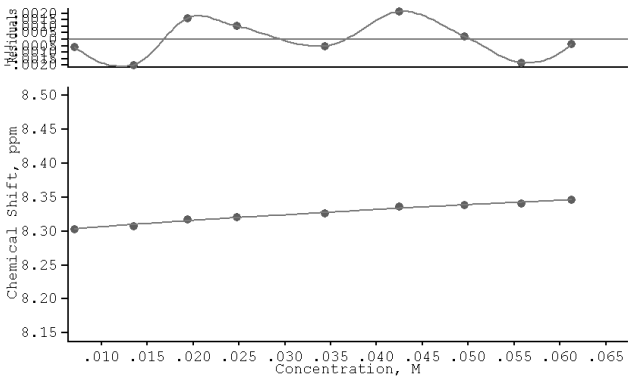

Figure S76 Binding curve from the ^{1}H NMR titration of receptor **10** with $TBANO_3$ in DMSO-d_5/ H_2O 0.5 % following the urea NH resonance at ~8.3 ppm. The data was fitted to a 1:1 biding model using WinEQNMR 2. $K_a < 10$ M^{-1}.

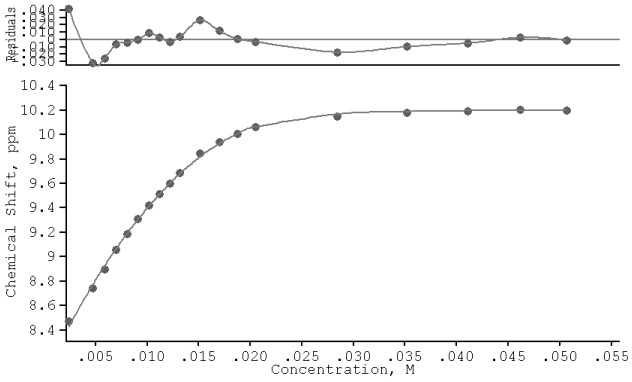

Figure S77 Binding curve from the ^{1}H NMR titration of receptor **10** with $TEAHCO_3$ in DMSO-d_5/ H_2O 0.5 % following the urea NH resonance at ~8.3 ppm. The data was fitted to a 1:2 binding model using WinEQNMR 2. $b_1 = K_1 = 1328$ M^{-1} (283.6), $b_2 = 870364$ M^{-2} (46370).

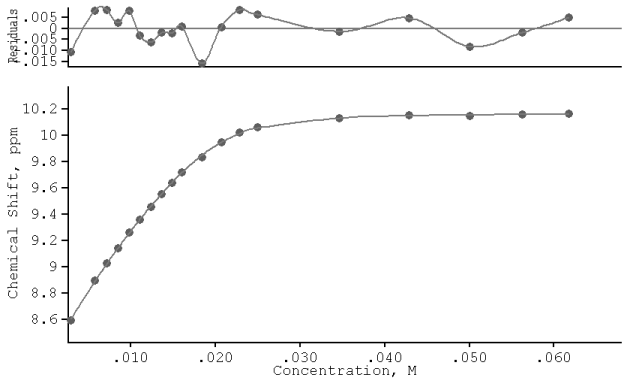

Figure S78 Binding curve from the ^{1}H NMR titration of receptor **10** with $TBAH_2PO_4$ in DMSO-d_5/ H_2O 0.5 % following the urea NH resonance at ~8.3 ppm. The data was fitted to a 1:2 binding model using WinEQNMR 2. $b_1 = K_1$ = 631 M^{-1} (65.27), b_2 = 52739 M^{-2} (14270).

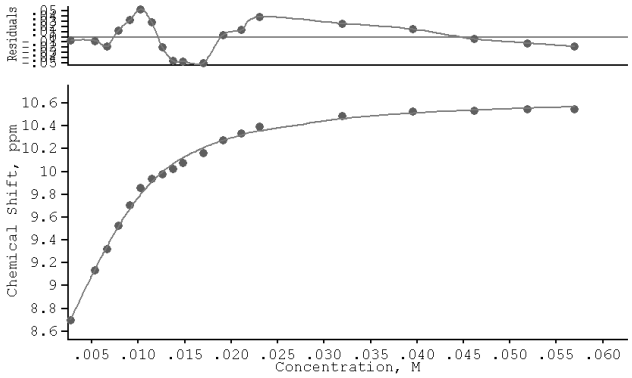

Figure A79 Binding curve from the ^{1}H NMR titration of receptor **10** with TBA_2SO_4 in DMSO-d_5/ H_2O 0.5 % following the urea NH resonance at ~8.3 ppm. The data was fitted to a 1:2 binding model using WinEQNMR 2. $b_1 = K_1$ = 3320 M^{-1} (651.3), b_2 = 411641 M^{-2} (66940).

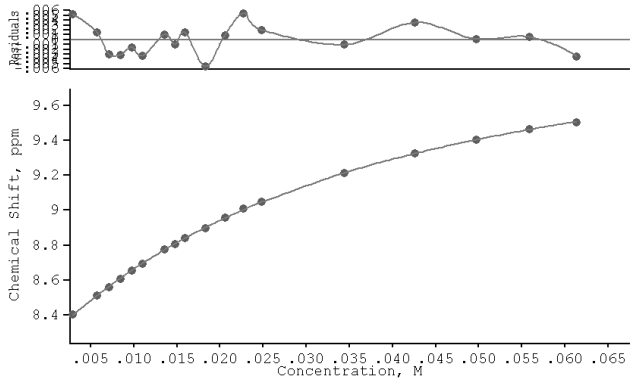

Figure S80 Binding curve from the ^{1}H NMR titration of receptor **11** with TBACl in DMSO-d_5/ H_2O 0.5 % following the urea NH resonance at ~8.3 ppm. The data was fitted to a 1:1 biding model using WinEQNMR 2. K_a = 32 M^{-1} (0.5787).

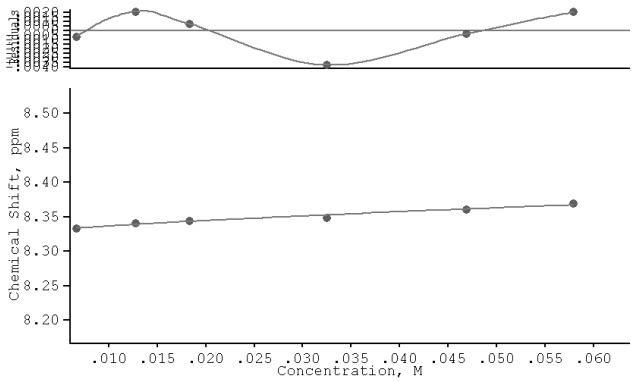

Figure S81 Binding curve from the ^{1}H NMR titration of receptor **11** with $TBANO_3$ in DMSO-d_5/ H_2O 0.5 % following the urea NH resonance at ~8.3 ppm. The data was fitted to a 1:1 biding model using WinEQNMR 2. K_a < 10 M^{-1}.

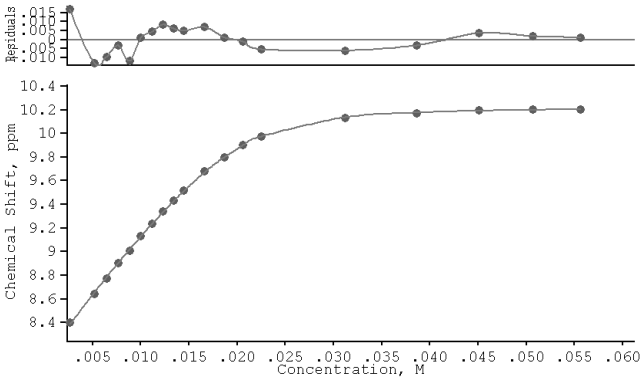

Figure S82 Binding curve from the ^{1}H NMR titration of receptor **11** with $TEAHCO_3$ in DMSO-d_5/ H_2O 0.5 % following the urea NH resonance at ~8.3 ppm. The data was fitted to a 1:2 binding model using WinEQNMR 2. $b_1 = K_1$ = 290 M^{-1} (28.62), b_2 = 246354 M^{-2} (14300).

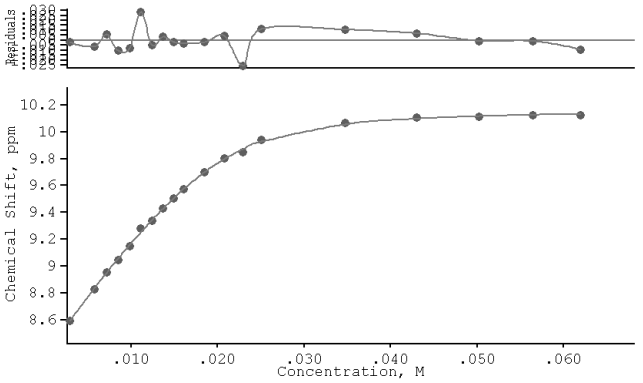

Figure S83 Binding curve from the ^{1}H NMR titration of receptor **11** with $TBAH_2PO_4$ in DMSO-d_5/ H_2O 0.5 % following the urea NH resonance at ~8.3 ppm. The data was fitted to a 1:2 binding model using WinEQNMR 2. $b_1 = K_1$ = 508 M^{-1} (118), b_2 = 206422 M^{-2} (22410).

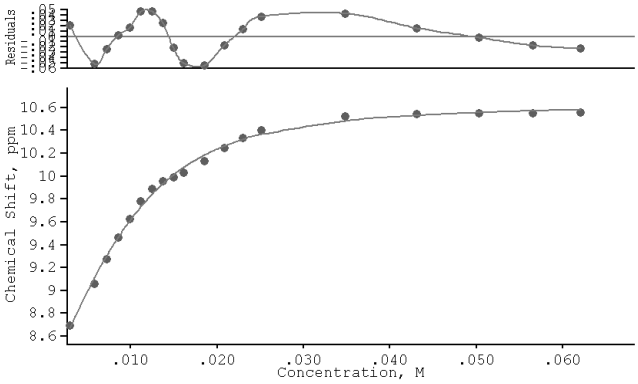

Figure S84 Binding curve from the ^{1}H NMR titration of receptor **11** with TBA_2SO_4 in DMSO-d_5/ H_2O 0.5 % following the urea NH resonance at ~8.3 ppm. The data was fitted to a 1:2 binding model using WinEQNMR 2. $b_1 = K_1 = 1267$ M^{-1} (345.3), $b_2 = 207037$ M^{-2} (47340).

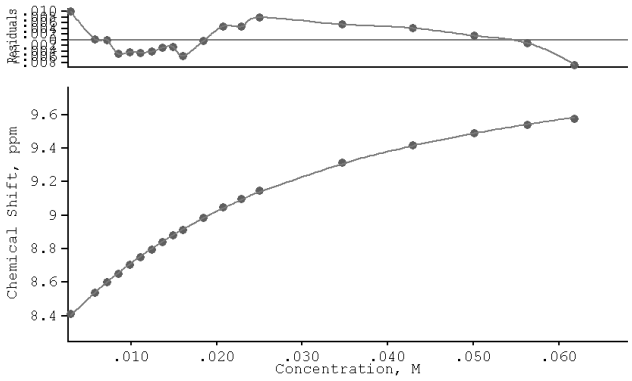

Figure S85 Binding curve from the ^{1}H NMR titration of receptor **12** with TBACl in DMSO-d_5/ H_2O 0.5 % following the urea NH resonance at ~8.3 ppm. The data was fitted to a 1:1 biding model using WinEQNMR 2. K_a = 44 M^{-1} (1.097).

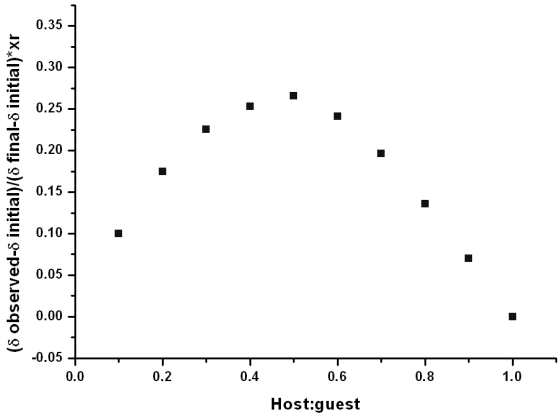

Figure S86 Job plot analysis for the interaction of receptor **12** with TBACl following the urea NH resonance at ~8.3 ppm.

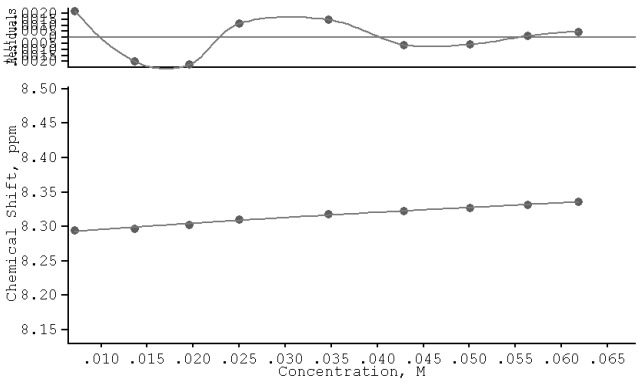

Figure S87 Binding curve from the ^{1}H NMR titration of receptor **12** with $TBANO_3$ in DMSO-d_5/ H_2O 0.5 % following the urea NH resonance at ~8.3 ppm. The data was fitted to a 1:1 biding model using WinEQNMR 2. $K_a < 10\ M^{-1}$.

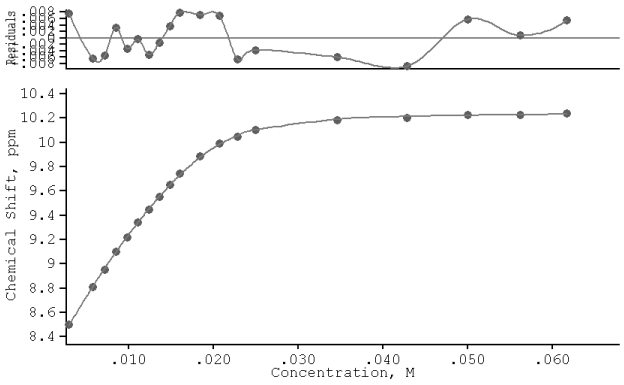

Figure S88 Binding curve from the ^{1}H NMR titration of receptor **12** with $TEAHCO_3$ in DMSO-d_5/ H_2O 0.5 % following the urea NH resonance at ~8.3 ppm. The data was fitted to a 1:2 binding model using WinEQNMR 2. $b_1 = K_1$ = 1026 M^{-1} (708.1), b_2 = 740068 M^{-2} (12680).

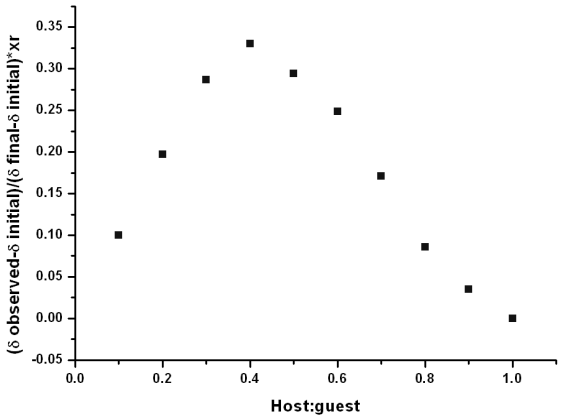

Figure S89 Job plot analysis for the interaction of receptor **12** with $TEAHCO_3$ following the urea NH resonance at ~8.3 ppm.

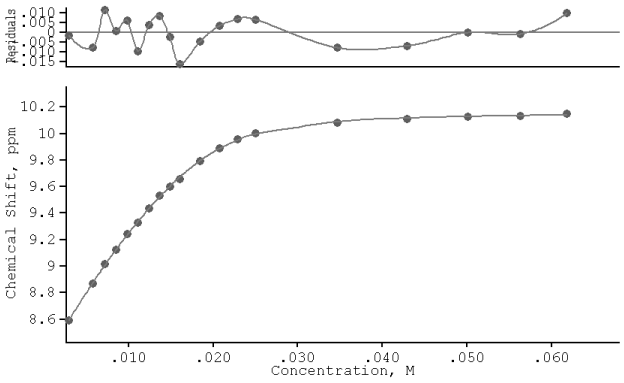

Figure S90 Binding curve from the ^{1}H NMR titration of receptor **12** with $TBAH_2PO_4$ in DMSO-d_5/ H_2O 0.5 % following the urea NH resonance at ~8.3 ppm. The data was fitted to a 1:2 binding model using WinEQNMR 2. $b_1 = K_1$ = 896 M^{-1} (79.49), b_2 = 447317 M^{-2} (21800).

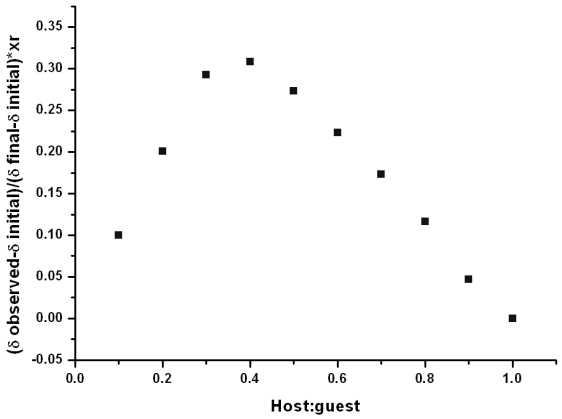

Figure S91 Job plot analysis for the interaction of receptor **12** with $TBAH_2PO_4$ following the urea NH resonance at ~8.3 ppm.

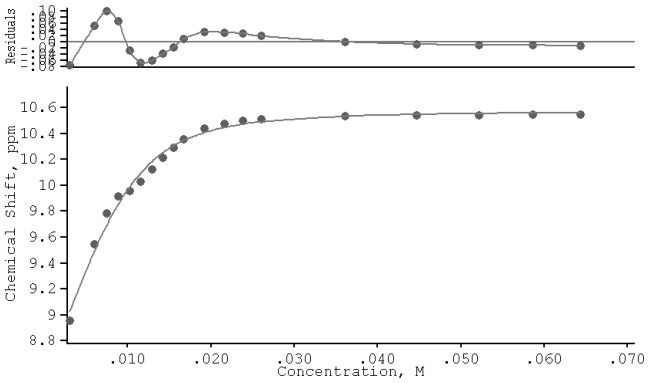

Figure S92 Binding curve from the ^{1}H NMR titration of receptor **12** with TBA_2SO_4 in DMSO-d_5/ H_2O 0.5 % following the urea NH resonance at ~8.3 ppm. The data was fitted to a 1:2 binding model using WinEQNMR 2. $b_1 = K_1 = 2296$ M^{-1} (202), $b_2 = 407788$ M^{-2} (82750).

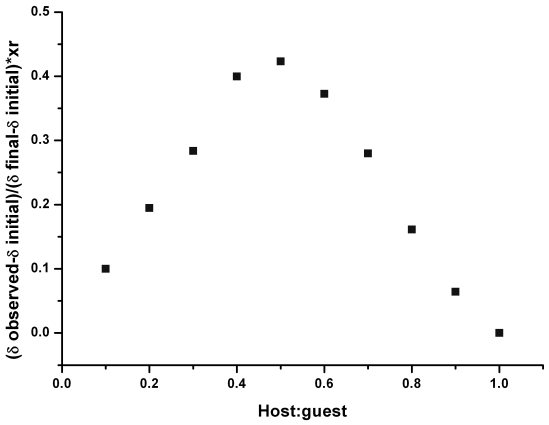

Figure S93 Job plot analysis for the interaction of receptor **12** with TBA_2SO_4 following the urea NH resonance at ~8.3 ppm.

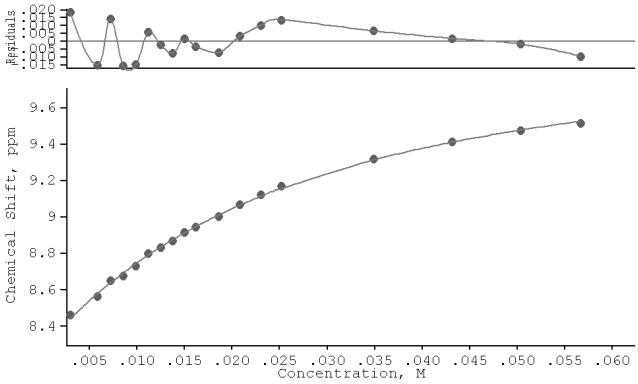

Figure S94 Binding curve from the ^{1}H NMR titration of receptor **13** with TBACl in DMSO-d_5/ H_2O 0.5 % following the urea NH resonance at ~8.3 ppm. The data was fitted to a 1:1 biding model using WinEQNMR 2. K_a = 49 M^{-1} (2.834).

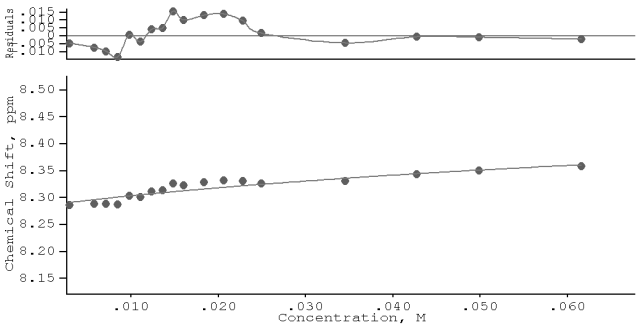

Figure S95 Binding curve from the ^{1}H NMR titration of receptor **13** with $TBANO_3$ in DMSO-d_5/ H_2O 0.5 % following the urea NH resonance at ~8.3 ppm. The data was fitted to a 1:1 biding model using WinEQNMR 2. K_a < 10 M^{-1}.

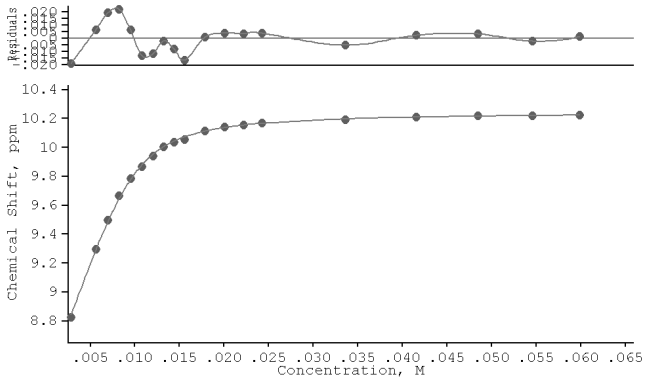

Figure S96 Binding curve from the ^{1}H NMR titration of receptor **13** with $TEAHCO_3$ in DMSO-d_5/ H_2O 0.5 % following the urea NH resonance at ~8.3 ppm. The data was fitted to a 1:1 biding model using WinEQNMR 2. K_a = 1521 M^{-1} (68.92).

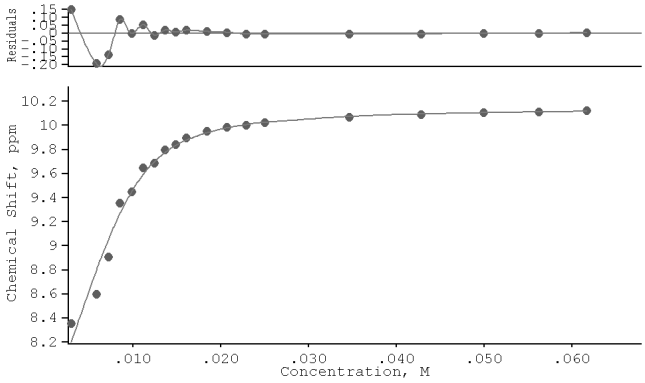

Figure S97 Binding curve from the ^{1}H NMR titration of receptor **13** with $TBAH_2PO_4$ in DMSO-d_5/ H_2O 0.5 % following the urea NH resonance at ~8.3 ppm. The data was fitted to a 1:1 biding model using WinEQNMR 2. K_a = 1273 M^{-1} (267.2).

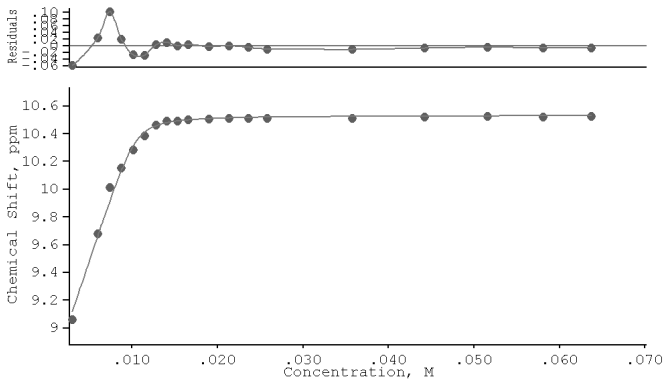

Figure S98 Binding curve from the ^{1}H NMR titration of receptor 13 with TBA_2SO_4 in DMSO-d_5/ H_2O 0.5 % following the urea NH resonance at ~8.3 ppm. The data was fitted to a 1:1 biding model using WinEQNMR 2. K_a = 8980 M^{-1} (185.4).

X-ray crystallography

In addition to the crystal structure reported in the main text, crystals of the oxalate complex of receptor **4** were grown by combining the receptor and an excess quantity of potassium oxalate in DMSO. To address the poor solubility of potassium oxalate in DMSO, 18-crown-6 was added and the solution was heated and filtered whilst hot. Slow evaporation of the resulting solution yielded crystals suitable for X-ray crystallography. The structure of the resulting complex is shown below.

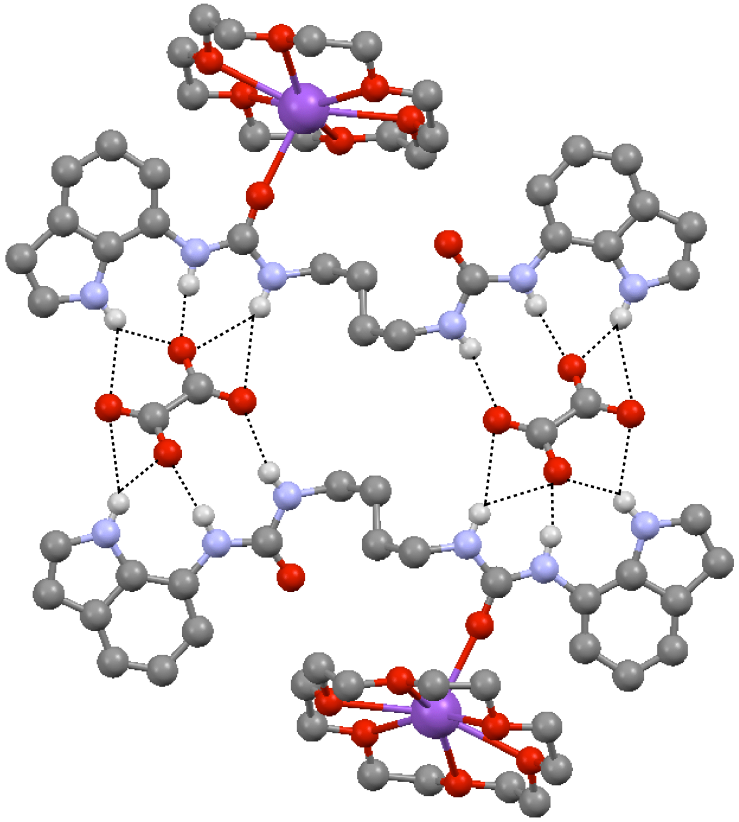

Figure S99 The X-ray crystal structure of the potassium oxalate/18-crown-6 complex of **4** showing a 2:2 binding mode. Non-acidic hydrogen atoms and additional K^+[18-crown-6] units have been removed for clarity.

The complex adopts a 2:2 receptor:anion stoichiometry, in which each oxalate anion is bound by 2 indolylurea units from 2 different receptors by a total of 9 hydrogen bonds. The NH···$O_{oxalate}$ bond lengths are in the range of 1.876 – 2.703 Å. The potassium

countercations are complexed within the cavity of the 18-crown-6 molecules. Two K^+[18-crown-6] units are bound to the urea C=O groups. The other two K^+[18-crown-6] units required for charge neutrality are coordinated between the layers of oxalate anions, as shown below.

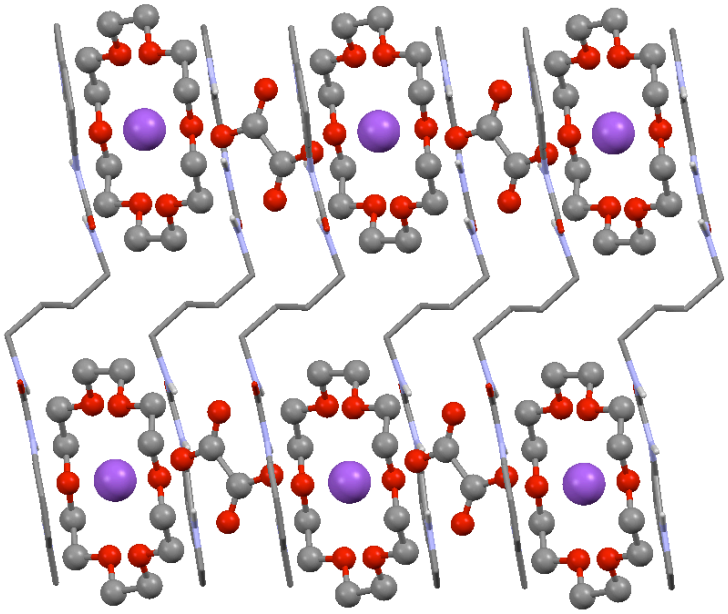

Figure S100 The crystal packing in the complex of **4** with potassium oxalate and 18-crown-6 showing the layering of K^+[18-crown-6] units between oxalate anions which are hydrogen bonded to the receptors.

This structure demonstrates that an interesting 2:2 binding mode is possible, although this finding does not necessarily indicate that such binding modes may be present in solution.

i. J. Wang, M. R. Wolf, J. W. Caldwell, P. A. Kollman, D. A. Case, *J. Comput. Chem.* 2004, **25**, 1157–1174.

ii. C. I. Bayly, P. Cieplak, W. Cornell, P. A. Kollman*, J. Phys. Chem.*1993, **97**, 10269.

iii. Gaussian 09, M. J. Frisch, G. W. Trucks, H. B. Schlegel, G. E. Scuseria, M. A. Robb, J. R. Cheeseman, J. J. A. Montgomery, T. Vreven, K. N. Kudin, J. C. Burant, J. M. Millam, S. S. Iyengar, J. Tomasi, V. Barone, B. Mennucci, M. Cossi, G. Scalmani, N. Rega, G. A. Petersson, H. Nakatsuji, M. Hada, M. Ehara, K. Toyota, R. Fukuda, J. Hasegawa, M. Ishida, T. Nakajima, Y. Honda, O. Kitao, H. Nakai, M. Klene, X. Li, J. E. Knox, H. P. Hratchian, J. B. Cross, V. Bakken, C. Adamo, J. Jaramillo, R. Gomperts, R. E. Stratmann, O. Yazyev, A. J. Austin, R. Cammi, C. Pomelli, J. W. Ochterski, P. Y. Ayala, K. Morokuma, G. A. Voth, P. Salvador, J. J. Dannenberg, V. G. Zakrzewski, S. Dapprich, A. D. Daniels, M. C. Strain, O. Farkas, D. K. Malick, A. D. Rabuck, K. Raghavachari, J. B. Foresman, J. V. Ortiz, Q. Cui, A. G. Baboul, S. Clifford, J. Cioslowski, B. B. Stefanov, G. Liu, A. Liashenko, P. Piskorz, I. Komaromi, R. L. Martin, D. J. Fox, T. Keith, M. A. Al-Laham, C. Y. Peng, A. Nanayakkara, M. Challacombe, P. M. W. Gill, B. Johnson, W. Chen, M. W. Wong, C. Gonzalez, J. A. Pople, Gaussian, Inc., Wallingford CT, 2009.

iv. AMBER11, D. A. Case, T. A. Darden, T. E. Cheatham-III, C. L. Simmerling, J. Wang, R. E. Duke, R. Luo, M. Crowley, R. C. Walker, W. Zhang, K. M. Merz, B. Wang, S. Hayik, A. Roitberg, G. Seabra, I. Kolossvary, K. F. Wong, F. Paesani, J. Vanicek, X. Wu, S. R. Brozell, T. Steinbrecher, H. Gohlke, L. Yang, C. Tan, J. Mongan, V. Hornak, G. Cui, D. H. Mathews, M. G. Seetin, C. Sagui, V. Babin, P. A. Kollman, University of California, San Francisco, 2010.

v. H. J. C. Berendsen, J. R. Grigera, T. P. Straatsma, *J. Phys. Chem.* 1987, **91**, 6269-6271.

vi. J.-P. Ryckaert, G. Ciccotti, H. J. C. Berendsen, *J. Comput. Phys.* 1977, **23**, 327–341.

vii. J. Weiser, P. S. Shenkin, W. C. Still, *J. Comput. Chem.*, 1999, **20**, 217–230.

viii. B. Jójárt and T. A. Martinek, *J. Comput. Chem.* 2007, **28**, 2051.

ix. L. Rosso, I. R. Gould, *J. Compt. Chem.* 2008, **29**, 24-37.

x. S. W. I. Siu, R. Vacha, P. Jungwirth, R. A. Böckmann, *J. Chem. Phys.* 2008, **128**, 125103.

xi. (a) I. Marques, "*Molecular modelling of transmembranar transporters for chloride*", MSc. Thesis, University of Aveiro, Portugal, 2011. (b) I. Marques, P. J. Costa, J. Sardinha, V. Félix, Nathalie Busschaert, M. Wenzel, P. A. Gale, manuscript in preparation.

xii. N. Kucerka, S. Tristram-Nagle, J. F. Nagle, *J. Membrane Biol.* 2005, **208**,193-202.

xiii. P. A. Hyslop, B. Morel, R. D. Sauerheber, *Biochemistry* 1990, **29**, 1025-1038.

xiv. B. Hess, C. Kutzner, D. van der Spoel, E. Lindahl, *J. Chem. Theory Comput.* 2008, **4**, 435-447.

xv. T. Darden, D. York, L. Pedersen, *J. Chem. Phys.* 1993, **98**, 10089-10092.

xvi. H. J. C. Berendsen, J. P. M. Postma, W. F. Vangunsteren, A. Dinola, J. R. Haak, *J Chem. Phys.* 1984, **81**, 3684-3690.

xvii. B. Hess, H. Bekker, H. J. C. Berendsen, J. G. E. M. Fraaije, *J. Comput. Chem.* 1997, **18**, 1463-1472.

18. M. J. Hynes, *J. Chem. Soc., Dalton Trans.*, 1993, 311-312.

19. N. J. Andrews, C. J. E. Haynes, M. E. Light, S. J. Moore, C. C. Tong, J. T. Davis, W. A. Harrel Jr., P. A. Gale, *Chem. Sci.*, 2011, **2**, 256-260.

20. D. Makuc, Triyanti, M. Albrecht, J. Plavec, K. Rissanen, A. Valkonen, C. Schalley, *Eur. J. Org. Chem.*, 2009, 4845-4866.